RF Project 3746

Technical Report 3746-1

the ohio state university research foundation
1314 kinnear road
columbus, ohio
43212

STUDIES OF HEAT SOURCE DRIVEN NATURAL CONVECTION

F. A. Kulacki and M. E. Nagle
Department of Mechanical Engineering
The Ohio State University
Columbus, Ohio 43210

and

Patrick Cassen
National Aeronautics and Space Administration
Theoretical Studies Branch
Moffett Field, California

NATIONAL AERONAUTICS AND SPACE ADMINISTRATION
Ames Research Center
Moffett Field, California 94035

Grant NGR 36-008-205

STUDIES OF HEAT SOURCE DRIVEN NATURAL CONVECTION

by

F. A. Kulacki and M. E. Nagle
Department of Mechanical Engineering
The Ohio State University
Columbus, Ohio 43210

and

Patrick Cassen
National Aeronautics and Space Administration
Theoretical Studies Branch
Moffett Field, California

Technical Report 3746-1

Grant NGR 36-008-205

August, 1973 - July, 1974

National Aeronautics and Space Administration
Theoretical Studies Branch
Ames Research Center
Moffett Field, California 94035

July, 1974

The Ohio State University Research Foundation
Columbus, Ohio 43212

FOREWORD

The work reported herein was sponsored by the National Aeronautics and Space Administration, Theoretical Studies Branch, Ames Research Center, Moffett Field, California under Grant NGR 36-008-205, by a Society of the Sigma Xi Grant-in-Aid of Research, and by the Department of Mechanical Engineering of The Ohio State University. The experimental study presented herein was conducted by one of the authors, (M. E. Nagle) in partial fulfillment of the requirements for the degree of Master of Science at The Ohio State University.

ABSTRACT

Natural convection energy transport in a horizontal layer of internally heated fluid with a zero heat flux lower boundary, and an isothermal upper boundary, has been studied for Rayleigh numbers from 1.58×10^5 to 2.5×10^9, which correspond to 114 to 1.8×10^6 times the critical value of linear stability theory analysis, respectively. Layer aspect ratios are kept small to minimize the effects of side walls on the steady state heat transfer measurements. Joule heating by an alternating current passing horizontally through the layer provides the volumetric energy source. The mean steady state Nusselt number at the upper boundary is determined by measuring the temperature difference across the layer and power input to the fluid.

Quantitative information on the time-mean temperature distribution and the fluctuating component of temperature about the mean temperature in steady turbulent convection are obtained from a small thermocouple inserted into the layer through the upper bounding plate. Data are also presented on the development of temperature at several vertical positions when the layer is subject to both a sudden increase and to a sudden decrease in power input. For changes of power input from zero to a value corresponding to a Rayleigh number much greater than the critical linear stability theory value, a slight hysteresis in temperature profiles near the upper boundary is observed between the heat-up and cool-down modes.

TABLE OF CONTENTS

LIST OF FIGURES

LIST OF FIGURES - CONTINUED

LIST OF TABLES

NOMENCLATURE

A	Area of heat transfer surface, cm^2
C	Constant of correlation for overall heat transfer
C_p	Specific heat at constant pressure of fluid, W-s/g-°C
D	Length of one side of convection cell, cm
f	Fraction error
Fo	Fourier number, $\alpha t/L^2$
g	Constant of gravitation acceleration corrected to latitude of The Ohio State University, 980.171 cm/s^2
H	Volumetric rate of energy generation in fluid, W/cm^3
k	Thermal conductivity of fluid, W/cm-°C
L	Vertical plate spacing, cm
L^*	Length scale defined by Eq. (19)
ℓ	Portion of fluid layer corresponding to unstable temperature distribution, cm
m	Constant of correlation for overall heat transfer
Nu_1	Nusselt number at upper boundary $$Nu_1 = \frac{\lvert \text{Power in} - \text{Power lost} \rvert}{k\,A} \frac{L}{T}$$
P	Power input to fluid, W
Pr	Prantdl number of fluid, ν/α
r	Coefficient of correlation
Ra_L	Rayleigh number $$Ra = \frac{g\beta}{\alpha\nu} L^3 \left(\frac{HL^2}{2k}\right)$$
ΔRa_L	Change of Rayleigh number impressed on fluid layer
t	Time, s

T'	Fluctuating temperature, °C
T	Mean fluid temperature, °C
ΔT	Temperature difference across fluid layer, °C
$\tilde{\Delta T}$	Destabilizing temperature difference, °C
V	Voltage, V
W	Weight percent of silver nitrate
z	Vertical coordinate in fluid layer, $0 \leq z \leq L$
Z	Nondimensional vertical coordinate in fluid layer, z/L

Greek Symbols

α	Thermal diffusivity of fluid cm^2/s
β	Isobaric coefficient of thermal expansion of fluid, $°C^{-1}$
δ_T	Thermal boundary layer thickness at upper surface, cm, L/Nu_1
μ	Dynamic viscosity of fluid, g-s/cm
ν	Kinematic viscosity of fluid, cm^2/s
ρ	Density of fluid, g/cm^3

Subscripts

c	Critical value
L/2	Based on a length scale of L/2
L	Based on a length scale of L
L*	Based on a length scale defined by Eq. (18)
o	Evaluated at z = o
ss	Steady state value
w	Evaluated at upper boundary, z = L
∞	Room temperature

Superscripts

$\frown$	Pertaining to overall heat transfer results, Ref. [16]
$*$	Indicates value of Nusselt number defined by Eq. (16)

SECTION I - INTRODUCTION

1.1 Exposition and General Discussion

Natural convection driven by a uniform internal energy source has not received a great deal of treatment in the literature despite its importance in engineering, geophysics, and astrophysics. For example, natural convection with distributed internal energy sources has been proposed to occur in the upper layers of the Earth's mantle [1,2,3] and has been offered as a mechanism to explain some of the surface features of our planet [4]. It is also currently believed that heat source driven natural convection is an important process in the evolution of all planetary interiors, including the Earth's moon for which a large body of data has recently become available [5]. It has also been postulated that thermal convection driven by internal heat release plays a role in energy transport in the outer region of stellar interior [6]. In connection with technological applications, the solution of engineering heat transfer problems in the chemical and food processing industries often centers on prediction of natural convection energy transport rates to the boundaries of confined fluids when an exothermic chemical reaction is present in the fluid. In the nuclear power industry, the analysis and prediction of both normal and failure mode heat transfer in LMFBR reactors requires a knowledge of free convection heat transfer in fluid systems with distributed heat sources.

Natural or free convection generally occurs when a large enough imbalance between buoyant forces tending to displace fluid elements and viscous forces tending to restrain fluid elements is caused to exist. Such buoyant forces are due to differences in density which are caused by some (destabilizing) temperature gradient in the fluid. For fluids satisfying the classical Boussinesq relation between density and temperature differences [7], the ratio of buoyant forces to viscous forces times the ratio of heat convected to heat conducted is the characteristic dimensionless parameter, and may be expressed by

$$Ra = \frac{g\beta}{\alpha\nu}\, \ell^3 \tilde{\Delta T} \,. \qquad (1)$$

This dimensionless group is called the Rayleigh number in honor of Lord Rayleigh who first used it in his analysis of hydrodynamic instability in horizontal fluid layers heated from below [8].

It is the purpose of this work to experimentally study natural convection driven by heat release from distributed volumetric energy sources in horizontal fluid layer with a constant temperature upper boundary and a zero heat flux lower boundary. Both boundaries in this study are rigid, zero velocity surfaces. The major objectives of the research were to obtain a correlation for steady state Nusselt number

versus Rayleigh number at the upper boundary and to investigate the nature of temperature field development when a step change in Rayleigh number is imposed. In addition, qualitative information was desired on the fluctuating component of temperature in steady turbulent convection at high Rayleigh number.

1.2 Subcritical Analysis

For Rayleigh numbers below the critical value at the onset of convection, the energy transport is by conduction. For a sufficiently thin fluid layer, the energy transport may be considered one-dimensional. In this case, the governing differential equation for the steady state temperature field is

$$\frac{d^2T}{dz^2} = -\frac{H}{k} . \tag{2}$$

The boundary conditions are $T = T_1$ = constant at $z = L$ and $dT/dz = 0$ at $z = 0$. Integrating twice and introducing the boundary conditions to evaluate the constants of integration gives the parabolic temperature distribution

$$T - T_1 = \frac{HL^2}{2k}\left(1 - \frac{z^2}{L^2}\right). \tag{3}$$

The Nusselt number at the wall ($z = L$) is given by

$$Nu_1 = \frac{L\left|dT/dz\right|_w}{T_{max} - T_w} \tag{4}$$

where $(T_{max} - T_w) = HL^2/2k$ and the derivative $\left|dT/dz\right|_w = HL/k$ from Eq. (3). For steady state one-dimensional conduction, the Nusselt number is, thus, a value of 2.

In the transient case of one-dimensional heat conduction, the partial differential equation governing the temperature field is

$$\frac{1}{\alpha}\frac{\partial T}{\partial t} = \frac{\partial^2 T}{\partial z^2} + \frac{H}{k} \tag{5}$$

with the boundary conditions

$$T = T_1 \text{ at } z = L \text{ and } t > 0$$

$$\partial T/\partial z = 0 \text{ at } z = 0 \text{ and } t > 0$$

$$T = T_1 \text{ at } t = 0 \text{ at } 0 \leq z \leq L .$$

This boundary-initial value problem was solved numerically in order to provide an estimate of the time required to reach steady state conduction after power was applied to an initially constant temperature layer. Such a time estimate provided a rough order of magnitude value for flow development time when convection was present. Numerical results from the solution of Eq. (5) for certain values of H used in this study are presented in Table B-VI.

1.3 Definition of Rayleigh Number

The Rayleigh number was defined by using the maximum temperature difference of conduction heat transfer, $HL^2/2k$, for the characteristic destabilizing temperature difference ΔT and the layer depth L, which corresponds to this temperature difference, as the length scale ℓ. These two physical quantities essentially scale the Rayleigh number to the specific rate of energy generation in the fluid which is a measurable quantity for all values of Rayleigh number. The Rayleigh number is, thus, given by

$$Ra_L = \frac{g\beta}{\alpha\nu} L^3\left(\frac{HL^2}{2k}\right) \qquad (6)$$

SECTION II - LITERATURE REVIEW

Only a few experimental studies of natural convection in internally heated fluid layers have been reported in the scientific literature. Some studies of natural convection in fluid layers heated from below are related to the present study and are, therefore, included in this literature review.

In 1967, Tritton and Zarraga [9] conducted flow visualization experiments in a volumetrically heated fluid layer with a rigid insulated bottom and a rigid insulated top. They were mainly concerned with a description of the cellular convection patterns for Rayleigh numbers in the vicinity of the critical value for the onset of motion. The developed cellular patterns for Rayleigh numbers up to eighty times the critical value of linear stability theory were in many respects similar to that for Benard convection [10] (i.e., for a fluid layer heated from below) but with the fluid descending in the cell centers and ascending at cell peripheries. The horizontal scale of the cell patterns was, in general, larger than that of Benard convection.

In 1968, Krishnamurti [11] experimentally studied the plan form of flow when a nonlinear temperature field existed in the conduction state in a fluid layer heated from below. It was found that when the mean temperature of the layer was changing at a constant rate, the static state was unstable to finite amplitude disturbances at Rayleigh numbers below the linear theory critical value. When the rate of temperature change was positive, the flow consisted of hexagons with downflow in the center; when this rate was negative, the flow consisted of hexagons with upflow in the center. A hysteresis in the heat flux at the layer boundaries was measured when the critical Rayleigh number was approached from above and then from below.

Whitehead and Chen [12] in 1970 experimentally investigated convection in an unstably stratified fluid layer bounded above by a free surface. Heating in the fluid was accomplished by thermally radiating the top few centimeters of the layer which produced a nonlinear mean temperature distribution there. Both thermocouple measurements and Schlieren photographs revealed that convection took the form of downward plunging jets of cool fluid from a region near the free upper surface. No energy transport measurements were obtained by Whitehead and Chen since they used layers of large vertical extent relative to the region of unstable stratification.

Schwab and Schwiderski [13], in 1971, reported observations of convection patterns for both developing and steady convection in an internally heated fluid layer similar to that of Tritton and Zarraga. Their apparatus was essentially the same as that of Tritton and Zarraga. Included in their experiments were observations of the evolution of cell patterns as steady state was reached. It was found that the flow development time depended strongly on the top and bottom boundary materials.

Their results were in substantial agreement with those of Tritton and Zarraga.

In 1973, Kulacki and Goldstein [14] reported an investigation of heat transfer in volumetrically heated fluid layer bounded by two rigid horizontal plates of constant and equal temperature. Correlations for mean heat transfer at the layer boundaries were obtained and it was found that for turbulent convection, the heat flux at the upper boundary was of the order of twice that at the lower boundary. Three regimes of convective flow were identified. Mean heat transfer data at the upper boundary were used to predict to with +10.7% the linear stability theory critical Rayleigh number [15]. The Rayleigh number in their study was defined by using L/2 as the characteristic length scale and $HL^2/8k$ as the characteristic destabilizing temperature difference. (The Rayleigh number used in this study is, thus, 32 times that of Kulacki and Goldstein.)

During the course of this work, a recent paper by Fiedler and Wille [16] was discovered in which energy transport in a horizontal fluid layer was investigated for the same boundary conditions, and in approximately the same range of Rayleigh number as reported herein. Both volumetric heating and heating from below was investigated in their study.

The apparatus of Fiedler and Wille consisted of a long, rectangular cell, 25 mm by 25 cm. The cell height was varied from 0.25 cm to 4.35 cm. The constant temperature top plate and zero heat flux bottom plate were constructed of copper and served as electrodes for passage of electric current through the fluid.

Fiedler and Wille reported a correlation for heat transfer in the form

$$\widehat{Nu}_1 = C\ \widehat{Ra}^m$$

where Nu was defined by

$$\widehat{Nu}_1 = HL^2/2k\Delta T$$

and Ra was defined by

$$\widehat{Ra}_L = \frac{g\beta}{\alpha\nu} L^3\Delta T\ .$$

Their experimental data yielded the correlation for overall heat transfer,

$$\widehat{Nu}_1 = 0.177\ \widehat{Ra}_L^{0.295} . \tag{7}$$

By redefining the Rayleigh and Nusselt numbers of Fiedler and Wille's study to conform to that of this work, the correlation (Eq. (7) becomes

$$Nu_1 = 0.526\ Ra_L^{0.228} . \tag{8}$$

It was suggested by Fiedler and Wille that in the case where the cell height, L, approaches infinity, a limiting value of the exponent, m, would be one-third when the Rayleigh number was defined in the usual way for Benard convection. Also, a dependence of Nusselt number on the Prandtl number was reported.

SECTION III - EXPERIMENTAL APPARATUS

3.1 Convection Cell

The convection cell (Figures 1-4) consisted of a horizontal fluid layer bounded above by a plate of constant temperature and bounded below by a plate of zero heat flux. The cell was 50.8 cm x 50.8 cm and the depth was varied from 2.54 cm to 12.7 cm by changing spacers between the two horizontal plates. The size of the cell was chosen to give the apparatus a range of Rayleigh number from 10^5 to 10^9 with moderate power input. Property values of pure water at 24°C were used to make preliminary design calculations.

Two of the side walls of the cell were 1.27-cm clear Plexiglas sheets and the other two side walls were formed by the electrodes for the passage of 60 Hz alternating current through the cell. The bottom plate was a 1.9 cm Plexiglas sheet machined square to ± 0.0127 cm. A micrometer and machinist square were used to make measurements.

The four side walls and bottom plate rested on another 1.27 cm Plexiglas sheet which acted as a foundation for the cell. In the bottom of this Plexiglas sheet were machined 41 grooves, 0.317 cm in diameter and 1.27 cm apart for the length of the cell. A 30-gauge nickel-chromium resistance heating wire was placed in these grooves. The total resistance of the heater was 473 Ω. The purpose of the heater was to counteract the conduction temperature gradient imposed by the warm fluid in the cell. Preliminary calculations to approximate the heat lost from the lower surface indicated that the heater power requirement would be less than 2 W.

Each of the electrodes was a silver-plated brass flat which extended the entire length and depth of the cell. The dimensions of the electrodes were 50.8 x 12.7 x 0.952 cm. Each electrode was machined flat to within ± 0.00254 cm and polished by hand to a mirror finish. A minimum thickness of 0.00254 cm silver plating was applied to the surface of the electrodes.

The top plate was machined from a T351-400 aluminum plate 2.54 cm thick. The plate was cut square to the dimensions of the cell minus 0.0762 cm on each side to allow room for the plate to slide into the cell. Eighteen channels were milled into the top plate in a double-pass spiral arrangement to allow cooling water to be circulated through the plate. The channels were 1.778 cm wide and 1.905 cm deep. The surface of the top plate was faced on a lathe to a flatness of less than ± 0.00254 cm. The thick, channeled plate was then covered with a 0.635 cm aluminum plate. Silicone rubber cement was spread onto the joints between the two plates, which were fastened together with brass machine screws, to prevent leakage. Finally, a 0.00762 cm thick sheet of Mylar was placed over the bottom and sides of the top plate to insulate it electrically from the current passing through the electrolyte

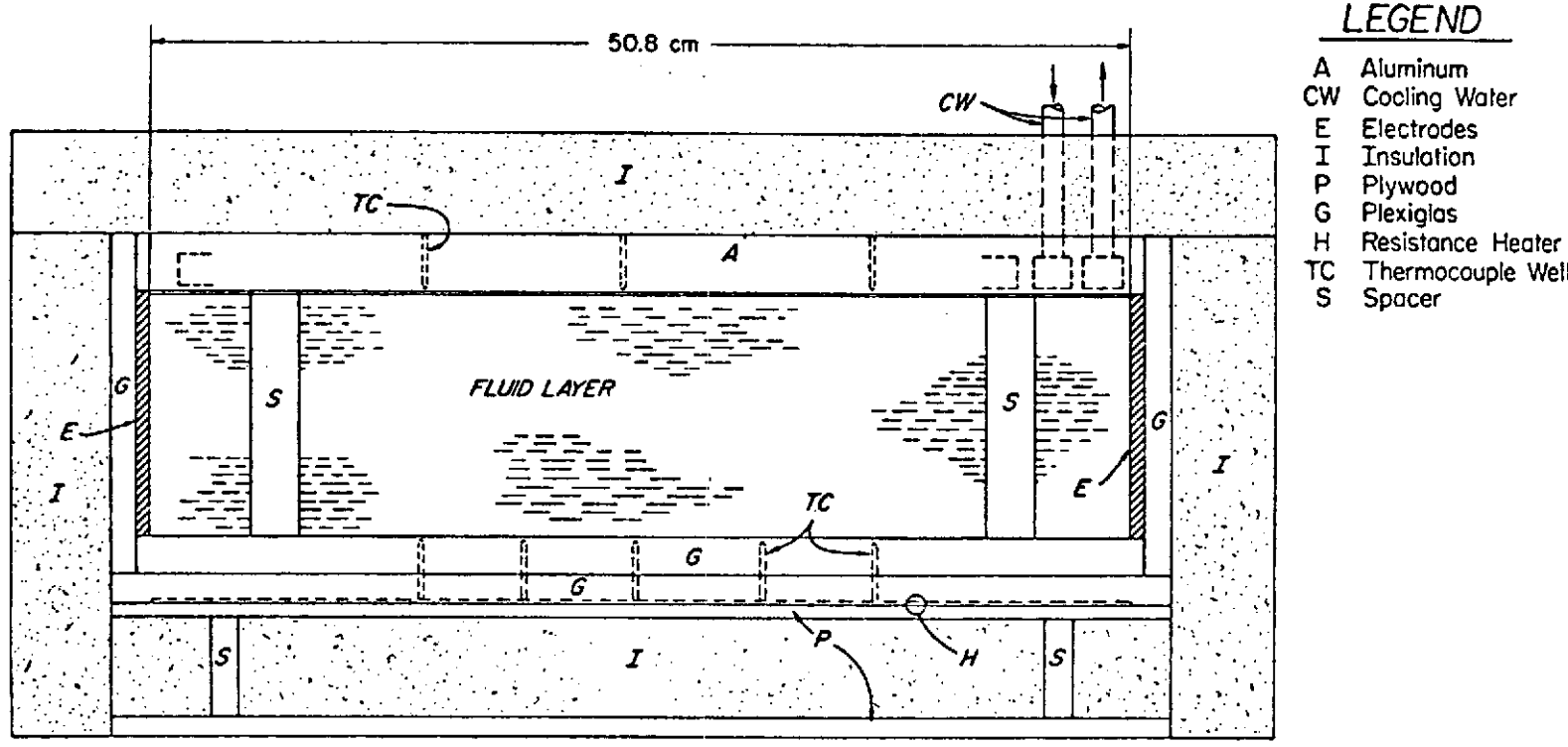

LEGEND

A	Aluminum
CW	Cooling Water
E	Electrodes
I	Insulation
P	Plywood
G	Plexiglas
H	Resistance Heater
TC	Thermocouple Well
S	Spacer

Figure 1. Detail View of Convection Cell

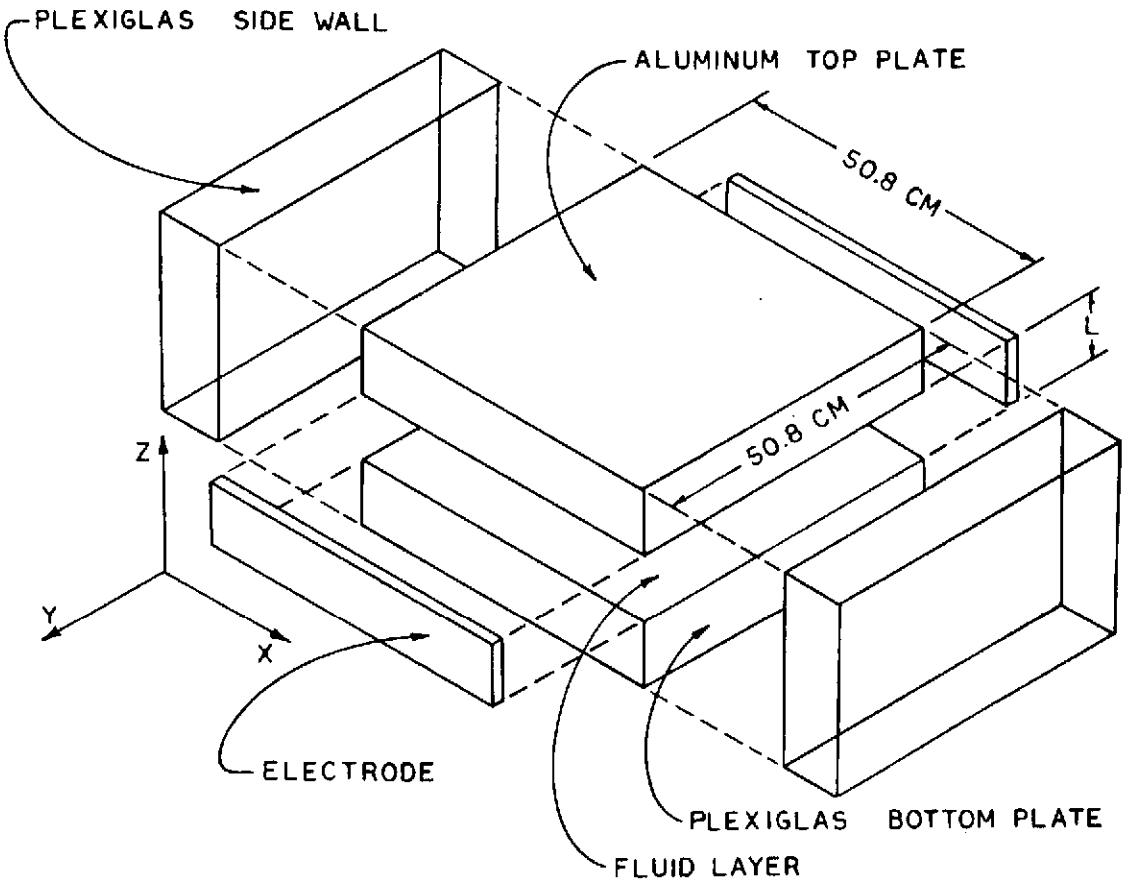

Figure 2. Assembly schematic of convection cell

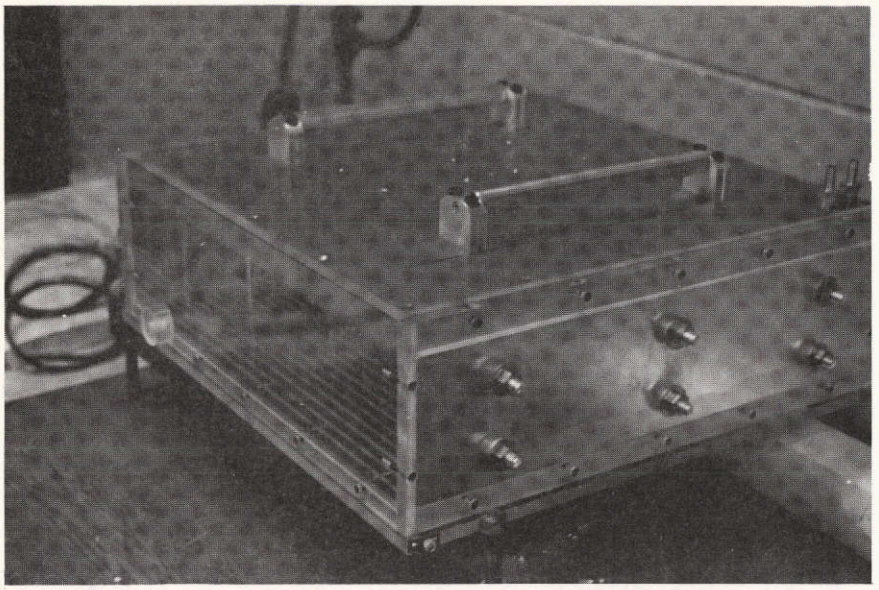

Figure 3. View of convection cell

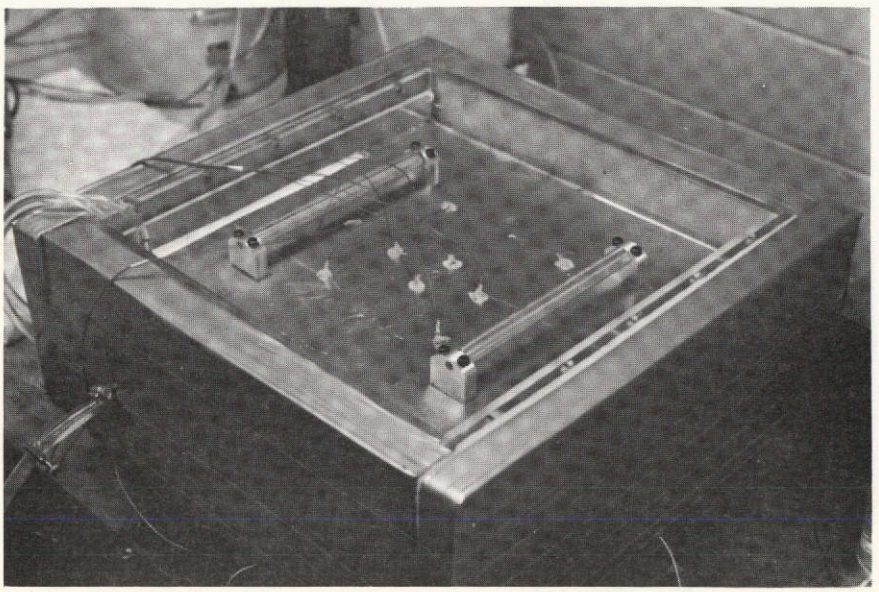

Figure 4. View of convection cell during experimental run

and to protect the aluminum from chemical attack by the silver nitrate in the fluid layer.

A numerical solution for the temperature distribution in the "constant temperature" plate [17] indicated that the periodicity in the plate surface temperature arising from the channels would be less than 0.001°C. This was considered negligible and the temperature across the plate was considered uniform.

When the plate was placed into the cell it rested on four spacers which were machined from 2.54 cm round, cast, Plexiglas rod. The spacers were made to a specified length to within ± 0.00127 cm tolerance.

The bottom and sides of the convection cell were insulated with fiberglass insulation board 5.08 cm thick. The thermal conductivity of the insulation was estimated to be 4.33×10^{-4} W/cm-°C. The insulation was fastened to the sides in a manner which enabled it to be removed easily, thus allowing inspection of the fluid layers through the two Plexiglas sidewalls.

The entire cell was placed on a triangular stand for leveling purposes. Leveling was accomplished by adjusting a screw at each of the three corners of the stand.

To make quantitative measurements of the transient temperature profile during the second part of the project, it was necessary to modify the cell slightly. This consisted of inserting a Plexiglas guide in the center of the top plate. This guide was necessary to allow insertion of a temperature sensing probe into the center of the cell while still preventing the aqueous silver nitrate solution from attacking the aluminum chemically.

3.2 Instrumentation and Other Apparatus

A schematic of the convection cell and instrumentation is shown in Figure 5. In order to accurately determine the Nusselt number it was necessary to measure the temperature difference between the top and bottom plates as accurately as possible. Temperature differences of 0.2°C were measured with confidence.

Copper-constantan thermocouple wire was used in construction of the thermocouples. All wire was taken from a single spool to ensure uniformity of all thermocouples. Junctions on the thermocouples were formed by arc welding in an inert argon atmosphere. One thermocouple was selected as a reference and all other thermocouples were compared to the reference output at the ice point and boiling point. The reference thermocouple was then calibrated against a high precision mercury thermometer. No resolvable difference in converted thermocouple output and temperature was detected.

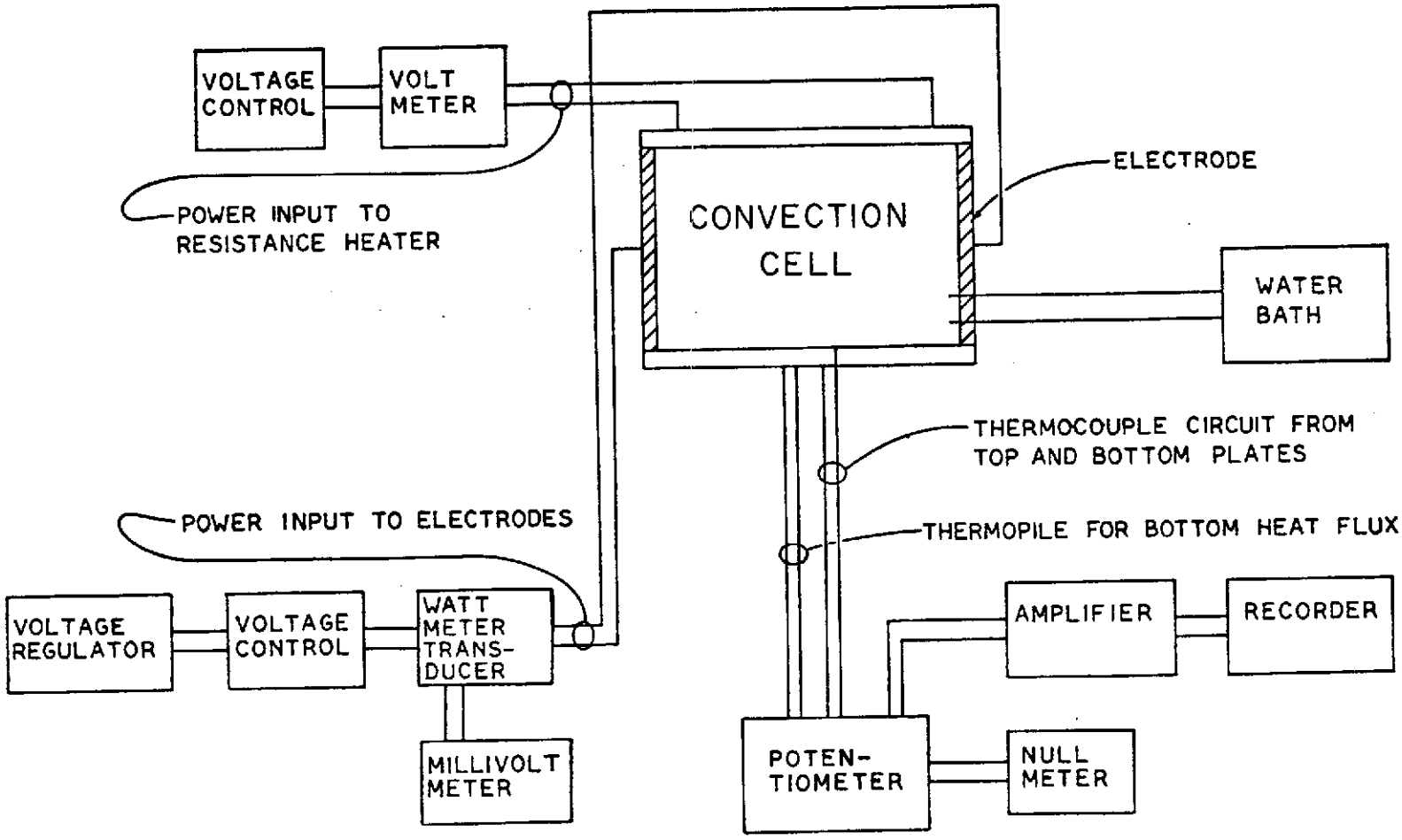

Figure 5. Schematic diagram of experimental apparatus

Thermocouple wells, each 0.32 cm in diameter, were drilled into the top and bottom plates to within 0.128 cm from the surfaces in contact with the fluid. The wells were spaced uniformly around the plate to obtain an averaged effect. All thermocouples were painted with General Electric No. 1202 insulating varnish. Thermocouples in the bottom plate were secured in their wells with epoxy cement; thermocouples in the top plate were secured in their wells with Teledyne, Technical "G" Copper Cement. The insulating varnish and copper cement produced a resistance of 10^7 Ω between the thermocouples and the aluminum top plate.

To measure the temperature difference across the layer, six thermocouples each in the top and bottom plates were connected in parallel. The output of each parallel circuit was determined relative to a reference thermocouple at 0°C. The difference in the two millivolt outputs determined in this way gave a reliable measurement of the temperature difference across the fluid layer.

The thermocouple arrangement for determining the heat flux through the bottom plate was a differencing thermopile using 20 thermocouples. Ten thermocouples were spaced across the bottom plates at 0.128 cm from the fluid surface and the other ten thermocouples were spaced across the bottom plate at 1.398 cm from the fluid surface. Thus, the output of the thermopile was interpreted as temperature difference across the material. This thermopile arrangement served as an indicator to determine when heat was being conducted into or out of the fluid layer through the lower surface.

A Leeds and Northrup type K-3 universal potentiometer, in conjunction with a Leeds and Northrup 9834 Electronic D-C null detector, was used to measure all thermocouple emf's. The published error of this arrangement is ± (0.015% of reading +0.5 μV). For measurements made in this study this would amount to ± 0.014°C.

A Sorenson Model 3000-S A-C voltage regulator was used to supply the power consumed in the fluid layer. The output of the voltage regulator was passed through a Variac so that regulation of power input to the cell could be achieved.

An electrical schematic of the fluid cell would appear as a capacitor-resistor-capacitor in series. Therefore, in calculating the power input to the electrodes, the impedance angle might be significantly greater than zero. For this reason, it was decided to use a wattmeter transducer for measuring power input. The transducer chosen was a F. W. Bell Model HX-2014W which uses a Hall element to take into account the impedance angle. The transducer was calibrated by the manufacture. A Fluke Model 8120-A digital readout multimeter was used to measure the output from the wattmeter transducer. This meter had a four and one-half digit display capacity and a published error of ± (0.05% of input +20 μV). For 50 W input to the fluid cell this would amount to ± 0.028 W. The instrument was certified by the manufacture to be within published specification.

A Lauda Model NB constant temperature bath was used to supply cooling water to the constant temperature top plate. Supply water temperature to the top plate did not vary from the desired setting by more than 0.1°C.

In the second part of the project it was desired to record a time trace of fluctuating temperatures. The temperature sensing probe consisted of a single 30 gauge copper-constantan thermocouple. The thermocouple was completely encased by pyrex glass in The Ohio State University glass shop to protect the thermocouple from chemical attack. The outside diameter of the glass tube containing the thermocouple was 0.19 cm and the thermocouple junction was 0.01 cm in diameter, nominally. The end of the glass tube was tapered to a very fine coating of glass around the thermocouple junction.

The thermocouple response was plotted on the output of the recorder by connecting the output of the glass encased thermocouple to a Hewlett Packard 7030A X-Y recorder and suddenly immersing the thermocouple into a container of warm water (Fig. 6). The time constant of the probe can be read directly from the recorded figure. Assuming a one degree of freedom system, the time constant is defined as the time required for the system to reach 63% of its asymptotic value. For the glass encased thermocouple used in this study the time constant is 0.7 second.

At a 7.62 cm plate spacing and a power input of 50 W, a temperature difference across the cell of nearly 1°C could be expected. This represents a change in thermocouple output of 41 μV for a copper-constantan thermocouple. In order to detect this small change in output with good resolution it was necessary to employ a Leeds and Northrup K-3 potentiometer in conjunction with a Leeds and Northrup 9835 microvolt amplifier. With this set-up a compensating emf corresponding to the lowest temperature in the system, the top plate, could be dialed into the potentiometer. Thus, the output to the amplifier was zero when the temperature probe was at the top plate temperature. However, when the probe was warmer than the top plate temperature, the difference between the temperature sensed by the probe and the top plate temperature was the output to the amplifier. The output of the amplifier was connected to a Honeywell Electronik 18 strip chart recorder. The published accuracy of this arrangement was ± 0.8% of range.

3.3 Experimental Procedure

Prior to each run, all reference thermocouples were placed in a 0°C ice bath and the interior portions of the convection cell were cleaned with demineralized water. The electrode surfaces were polished with silver polish and were then wiped clean with acetone to remove any residue.

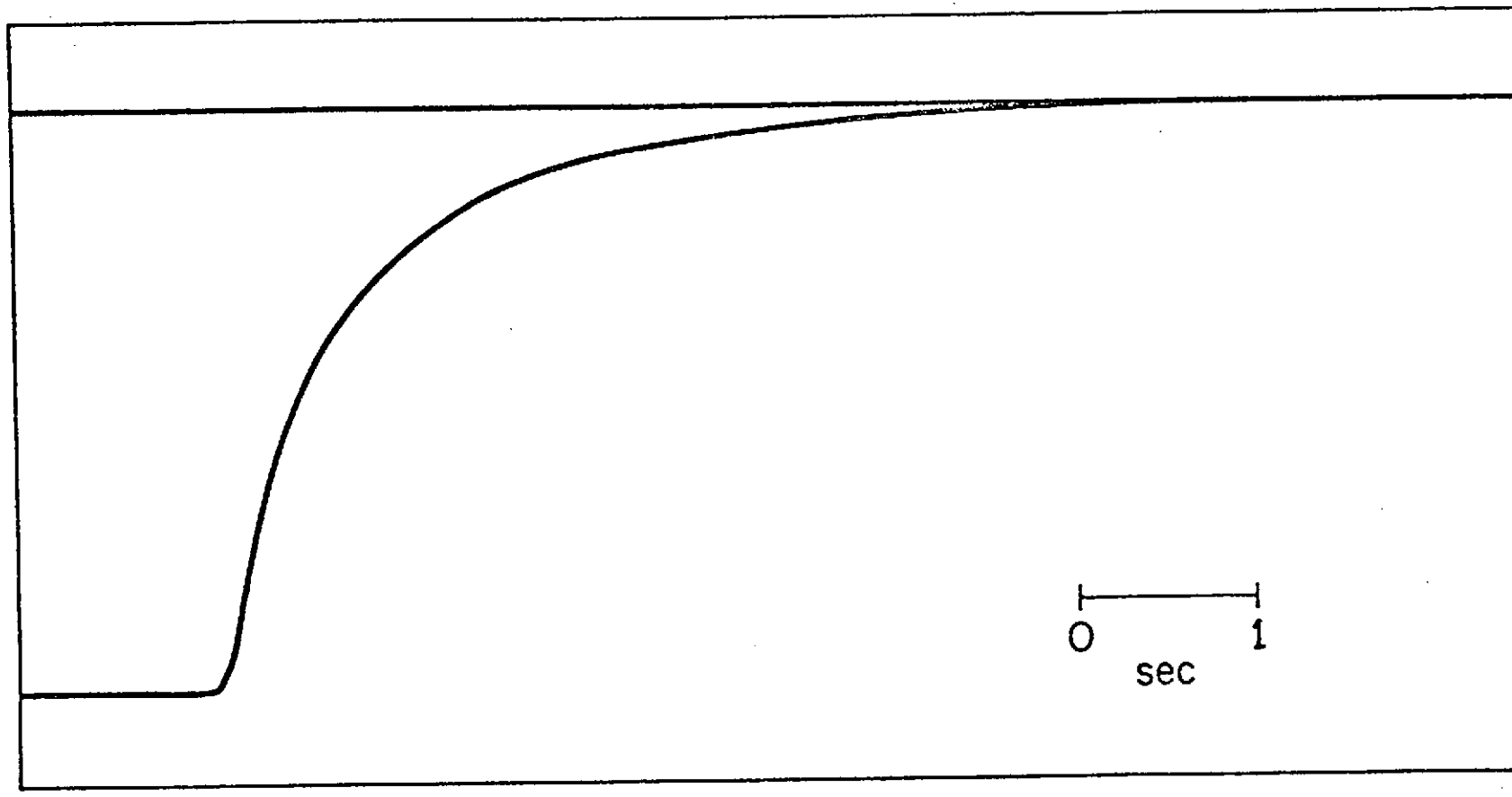

Figure 6. Response of thermocouple probe to a 1°C change in temperature

The initial horizontal alignment of the convection cell was accomplished by adjusting the legs on the triangular stand on which the cell rested. Fine horizontal alignment was accomplished with the Fell precision level placed on top of the bottom plate. The sensitivity of this level was 0.00416 cm/m.

The four Plexiglas spacers were spaced around the cell at the corners to support the top plate. The convection cell was then filled at a very slow rate with demineralized water to a level even with the top of the spacers. A conductivity meter attached to the top of the demineralizer indicated the specific resistance of the demineralized water was greater than 10^6 Ω. The desired quantity of reagent grade silver nitrate crystals were measured out with an analytical balance to ±0.001 g and then dissolved in the demineralized water. Because of the large quantity of water in the fluid layer, the convection cell was used as a mixing chamber for forming the silver nitrate solution. Since Rayleigh numbers in this study were greatly in excess of the critical value and most of the mean heat transfer measurements were in the turbulent regime, any nonuniformities in the concentration of silver nitrate would be minimized by convective mixing within the layer. In addition, the long flow development time needed for mean heat transfer measurements with large plate spacings would act in favor of reducing nonuniformities in silver nitrate concentration. The concentration of silver nitrate crystals was kept to approximately 0.02 M.

The top plate was brushed with melted paraffin at its corners and at any other apparent breaks in the Mylar film to ensure that no fluid would come in contact with the aluminum top plate. The top plate was then eased very carefully into the convection cell. When the plate came into contact with the top surface of the fluid it was tilted slightly at an angle and then allowed to settle down flat on top of the spacers. It was necessary to tilt the plate in this manner to allow trapped air bubbles to escape.

After placing the insulation on the sidewalls the power was turned on. The output from the wattmeter transducer was used to adjust the voltage across the electrodes to where the desired power input was obtained. The power consumed varied from 180 W for the 12.7 cm plate spacing to 7.2 W for the 2.54 cm plate spacing. The method of adjusting the voltage across the resistance heater on the bottom was developed by trial and error.*

After a time has elapsed much greater than that required by the pure conduction model to reach equilibrium, the temperature of the top and bottom plates was determined. At least four readings of temperature for each plate was collected and averaged. Normally another set of four

*The formula $V = 14(T_O - T_\infty)$ proved to be a good guide but fine adjustments were made previous to a final reading of data.

readings were collected and averaged one-half hour later in order to ensure that equilibrium had been obtained. When good agreement was reached the data was recorded.

In the second part of the project, the problem of determining the transient temperature distribution, the preliminary procedure for making the cell ready to turn on the power was the same as described above. After all instruments had had sufficient time to warm-up, the potentiometer was standardized using the meter on the amplifier as a null meter. The temperature of the top plate was measured using the thermocouples embedded in the aluminum plate again using the amplifier as a null meter.

After selecting the desired amplifier scale and strip chart speed the glass encased thermocouple was placed into the cell through the Plexiglas guide. The depth of the thermocouple was measured with a vernier caliper accurate to 0.01 cm. A compensating voltage of opposite polarity to that of the thermocouple and of magnitude sufficient to place the recorder pen at approximately 30% of full scale was dialed into the potentiometer. The power was turned on and thermocouple output was recorded as a function of time until steady state convection was reached at that particular depth in the fluid cell. After steady state was obtained, the power was turned off and again the thermocouple output was recorded as a function of time until a constant temperature was obtained at that particular depth in the fluid cell. This procedure was repeated at various depths in the fluid layer. In this manner it was possible to construct a family of temperature profiles at various times in the transition to steady state for both warm-up and cool-down of the layer.

When steady state convection was obtained, the apparatus, set up as described above, was used to record the instantaneous temperature at the thermocouple position on the strip chart. This output was used to determine characteristics of the fluctuating component of temperature.

SECTION IV - PRESENTATION OF RESULTS

4.1 Steady State Heat Transfer Measurements

Results of heat transfer measurements for each run are given in tabular form in Tables B-I and B-II and are presented graphically in Figure 7.

The Nusselt number was defined using the depth of the fluid layer, L, as the characteristic length scale and the measured temperature difference between top and bottom plates as the characteristic temperature difference. In terms of the power dissipated within the layer, the Nusselt number is given by

$$Nu_1 = \frac{(\text{Power in} - \text{Power lost})\ L}{k\ A\ (T_0 - T_1)}. \tag{9}$$

The power lost is that due to free convection effects to the environment and was computed using standard correlations [17]. Using a least squares curve fit, the Rayleigh number and Nusselt number were first correlated assuming a relation of the form

$$(Nu_1 - 2) = C(Ra_L - Ra_{L,c})^m \tag{10}$$

where $Ra_{L,c}$ is given by linear stability theory [15] as 1386. The resulting correlation was

$$(Nu_1 - 2) = 0.138(Ra_L - 1386)^{0.277 \pm 0.005} \tag{11}$$

$$1.5 \times 10^5 \leq Ra_L \leq 2.5 \times 10^5$$

$$6.21 \leq Pr \leq 6.64$$

$$0.05 \leq L/D \leq 0.25$$

$$r = 0.992,\ 36 \text{ observations}$$

where r is the coefficient of correlation.

In addition, the more conventional correlation form

$$Nu_1 = C\ Ra_L^m \tag{12}$$

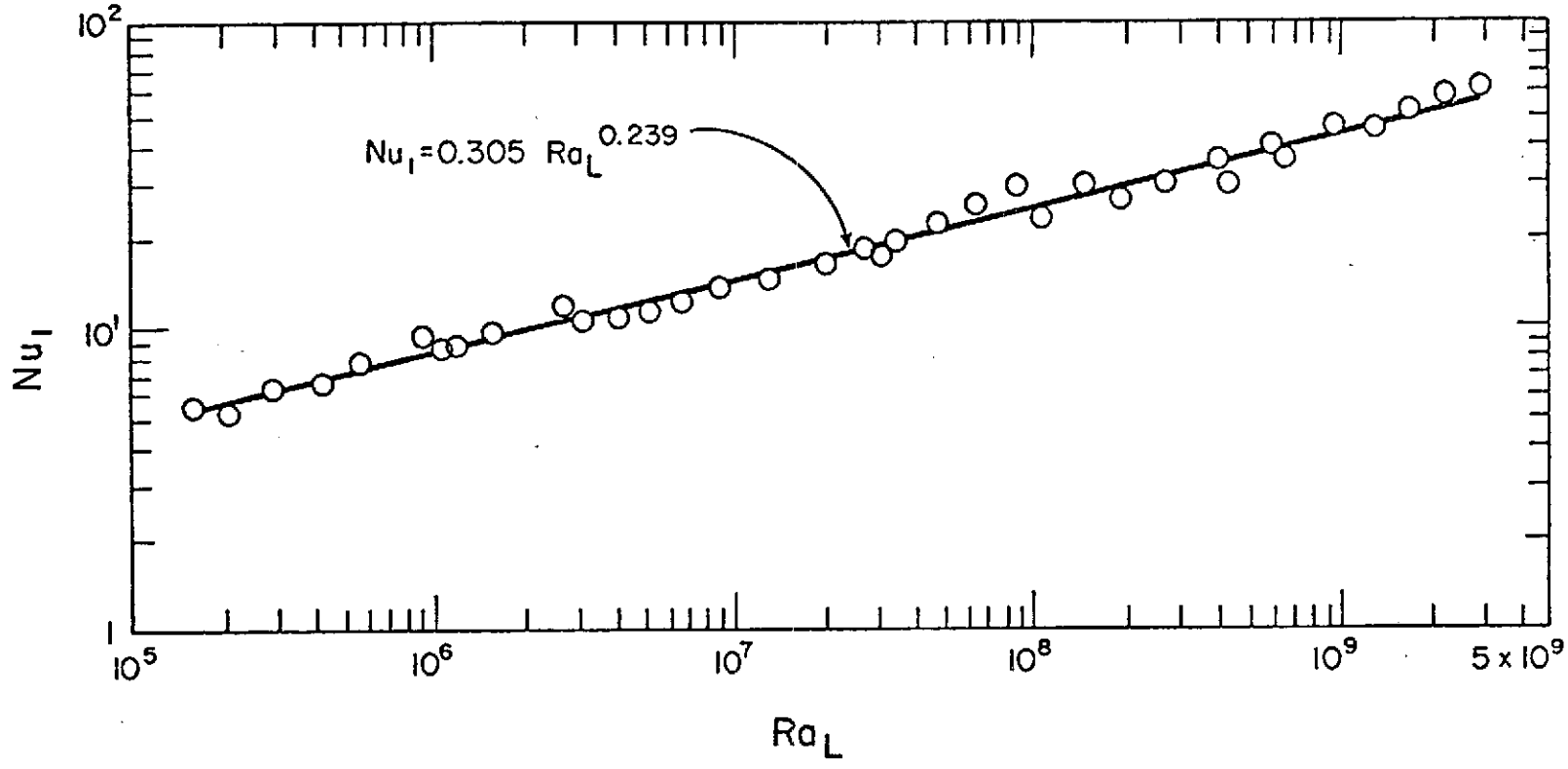

Figure 7. Overall heat transfer results for steady convection

$Nu_l = hL/k$, $Ra_L = (g\beta/\alpha\nu) L^3 (HL^2/2k)$

was computed. The resulting correlation, using all data points was

$$Nu_1 = 0.305\ Ra^{0.239 \pm 0.005} \tag{13}$$

$$1.5 \times 10^5 \leq Ra_L \leq 2.5 \times 10^9$$

$$6.21 \leq Pr \leq 6.64$$

$$0.05 \leq L/D \leq 0.25$$

$$r = 0.995,\ 36 \text{ observations.}$$

The data are almost as well represented by a correlation of the form

$$Nu_1 = (0.25 \pm 0.004)Ra_L^{0.25} \tag{14}$$

for the same range of Ra_L, Pr and L/D as for Eq. (13).

Finally, data for which the temperature difference between the top and bottom plates was less than 1°C were selected and correlated to the form Eq. (12). This was done to provide a correlation for which any nonlinear effects in thermophysical property values would be at a minimum and for which the requirements of the Boussinesq equation of state would be more nearly satisfied [7]. The resulting correlation using the selected data points was

$$Nu_1 = 0.375\ Ra_L^{0.225 \pm 0.008} \tag{15}$$

$$1.5 \times 10^5 \leq Ra_L \leq 1.9 \times 10^8$$

$$6.52 \leq Pr \leq 6.64$$

$$r = 0.991,\ 16 \text{ observations.}$$

Assuming that the correlation of Ra_L with Nu_1 in the form Eq. (12) holds in the vicinity of the critical point, it can be used to determine the critical Rayleigh number by extrapolation to the conduction value of Nu_1 of 2.0. This assumes that the physics of the fully developed convection at high Ra_L is the same as that in the post-stability regime. This is probably not the case. However, by extrapolating Eq. (13) to a Nusselt number of 2, a critical Rayleigh number of 2614

is predicted. By extrapolation of Eq. (15) the conduction value of Nusselt number, a critical Rayleigh number of 1702 is predicted, which is within 23% of the linear stability theory prediction.

The ratio of the actual temperature difference in the fluid layer and the temperature difference of pure conduction was plotted against the Rayleigh number (Fig. 8). From Figure 8 it is seen that the actual fluid temperature difference varied between 3% and 35% of the pure conduction temperature difference over the range of Ra_L in this study.

The correlation for mean heat transfer of this study Eq. (13) is at variance with that of Fielder and Wille [16] but is in good agreement with that of Kulacki and Goldstein [14] for heat transfer at the upper boundary of an internally heated fluid layer with two constant temperature surfaces. Fielder and Wille's results, in terms of the definition of Nu_1 and Ra_L, are again

$$Nu_1 = 0.526\ Ra_L^{0.228} \tag{8}$$

$$2 \times 10^5 \leq Ra_L \leq 6 \times 10^8$$

$$0.29 \leq L/D \leq 1.65.$$

This correlation gives values of Nu_1 considerably greater than Eq. (13). Since the data of Fiedler and Wille was for fluid layers with aspect ratios greater than 0.25 in a convection cell of 25 mm by 25 cm, it is entirely possible that the sidewalls of their cell has a marked effect on convection by aiding the development of a gross circulation pattern within the layer at high Rayleigh number. In the present study, however, the large horizontal extent of the layer minimizes the effects of such secondary flow due to sidewalls on the vertical energy transport in the central region of the layer.

An interesting comparison can be made between the results of the present study and those of Kulacki and Goldstein [14]. It should be recalled that the correlations of Kulacki and Goldstein were for internally heated fluid layers with two constant temperature surfaces while that of the present study are for a layer with a zero heat flux lower boundary. Convection in the layer of the present study can be considered to represent convection in that portion of a layer with two isothermal surfaces which accounts for the heat transport at the upper boundary. Thus, a comparison of the upward heat flux results of Kulacki and Goldstein to those of the present study requires a redefinition of the length scale of the Rayleigh number.

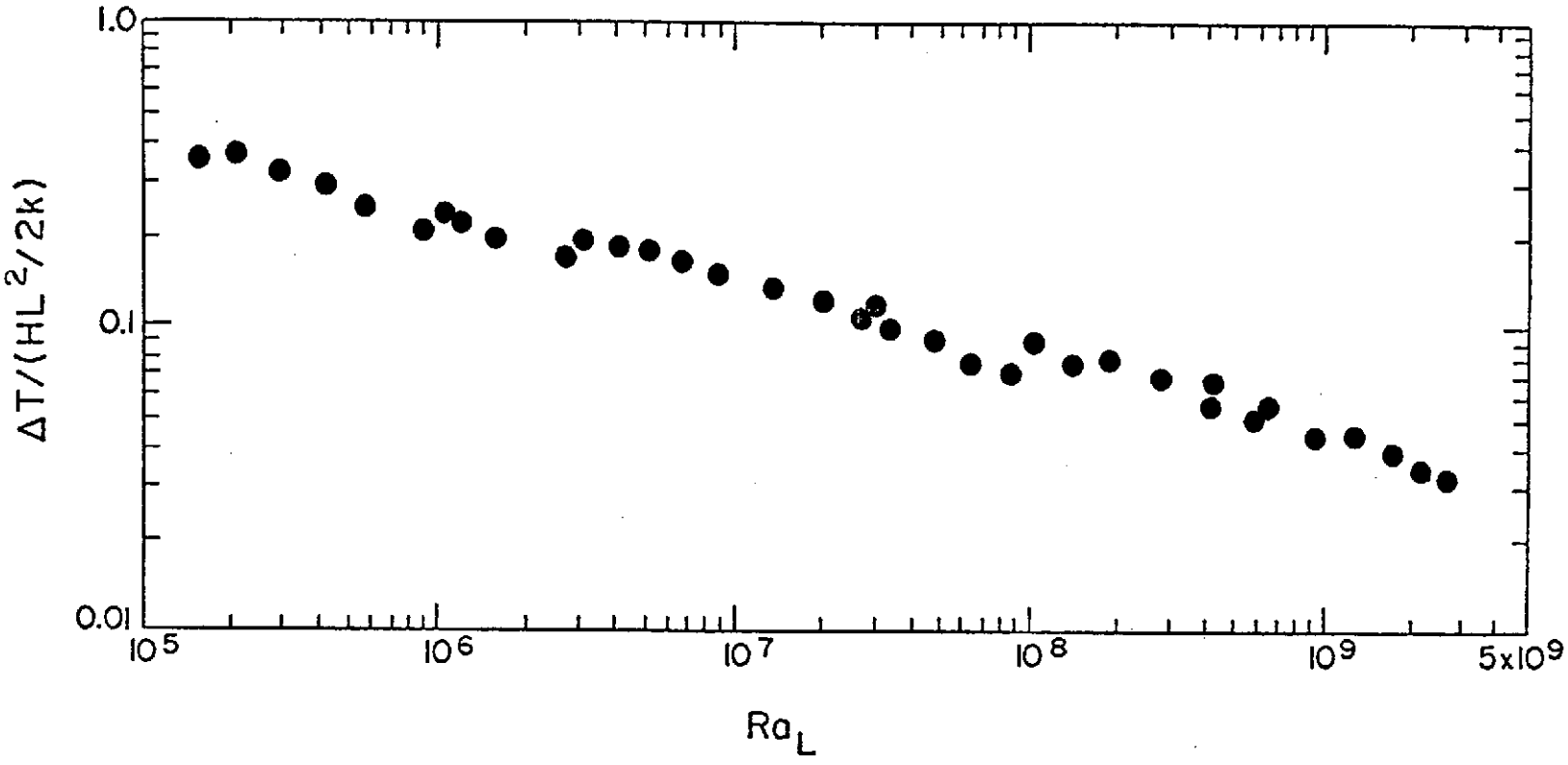

Figure 8. Actual temperature difference across layer as a function of Rayleigh number in steady convection. $T = T_0 - T_1$. $Ra_L = (g\beta/\alpha\nu)L^2(HL^2/2k)$

First, a new Nusselt number is defined as

$$Nu_1^* = Nu_1/Nu_{1,c} \tag{16}$$

where $Nu_{1,c}$ is the conduction value (or critical value) of Nusselt number. ($Nu_{1,c} = 2$ for the present study and $Nu_{1,c} = 4$ for a layer with two equal temperature boundaries.) Next, consider that in a layer with two isothermal boundaries of equal temperature, the upward heat transfer corresponds to the fraction of the energy generated within the layer given by the ratio

$$\frac{Nu_1^*}{Nu_1^* + Nu_0^*} = \frac{\text{heat transfer at upper boundary}}{\text{total heat transfer}}. \tag{17}$$

This ratio is used to define the vertical distance, L^*, from the upper boundary to a plane of essentially zero average heat flux within the layer. The distance L^* is given by

$$\frac{L^*}{L} = \frac{Nu_1^*}{Nu_1^* + Nu_0^*}. \tag{18}$$

With the correlations of Kulacki and Goldstein wherein the Rayleigh number is redefined in terms of the layer depth L, Eq. (18) becomes

$$\frac{L^*}{L} = \frac{0.0969\ Ra_L^{0.236}}{0.0969\ Ra_L^{0.236} + 0.381\ Ra_L^{0.094}}. \tag{19}$$

If a value of Ra_L is specified, then from Eq. (19) a value of L^* can be found. This value of L^* is then used in Eq. (13) for the length scale in the Rayleigh and Nusselt numbers.

Table I lists values of Nusselt numbers computed with the modified correlations of Kulacki and Goldstein and the present study. From Table I, it can be seen that Eq. (13) predicts Nusselt numbers somewhat larger than those of the Kulacki-Goldstein correlation for Rayleigh numbers greater than 10^6. However, the agreement here is considered good since the Rayleigh number range of the present study extends considerably beyond that of the Kulacki-Goldstein correlation. Furthermore, the plane of zero average heat flux in the layer with two isothermal boundaries is not hydrodynamically the same as the rigid, zero heat flux lower boundary of the present study.

Table I - Comparison of Nusselt Numbers for Upward Heat Flux of the Present Study and the Correlation of Kulacki and Goldstein [14]

Kulacki and Goldstein				This Study	
Ra_L	Nu_1^*	Nu_0^*	L^*/L	Ra_L^*	$Nu_{L^*,1}^*$
10^5	1.46	1.13	0.565	5.6×10^3	1.20
10^6	2.24	1.39	0.616	8.84×10^4	2.35
10^7	3.83	1.73	0.688	1.55×10^6	4.61
10^8	6.60	2.15	0.754	2.44×10^7	8.90
10^9	11.43	2.67	0.812	3.54×10^8	14.35

As the mean heat transfer data covered a fairly large range of Rayleigh number, it seemed appropriate to analyze the data for the existence of the so-called "discrete transitions" in heat flux, which have been reported for natural convection in fluid layers heated from both below and from within [14,15,18,19]. Such transitions appear on a linear plot of Nusselt number times Rayleigh number versus Rayleigh number over a limited range of Rayleigh numbers as a sudden change in the slope of straight line segments fit to the data. It is the nature of the plot to smooth the data in a way that accentuates inflections in the slope of the curve. The Rayleigh numbers at the abrupt changes in the slope of the curve are termed "transition Rayleigh numbers."

Five transition Rayleigh numbers were found with the data of this study. They are depicted in Figures 9 to 13 and summarized below in Table II. Table II also contains transition Rayleigh numbers at the upper boundary reported by Kulacki and Goldstein.

Table II - Transition Rayleigh Numbers

This Study		Kulacki and Goldstein	
Ra_L	$Ra_L/Ra_{L,c}$ ($Ra_{L,c} = 1386$)	$Ra_L/2$	$Ra_{L/2}/Ra_{L/2,c}$ ($Ra_{L/2,c} = 560$)
4.2×10^5	3.03×10^2	1.2×10^4	0.21×10^2
4.9×10^6	3.54×10^3	9.2×10^4	1.64×10^2
3.05×10^7	2.20×10^4	1.95×10^5	3.48×10^2
4.0×10^8	2.89×10^5		
1.4×10^9	1.01×10^6		

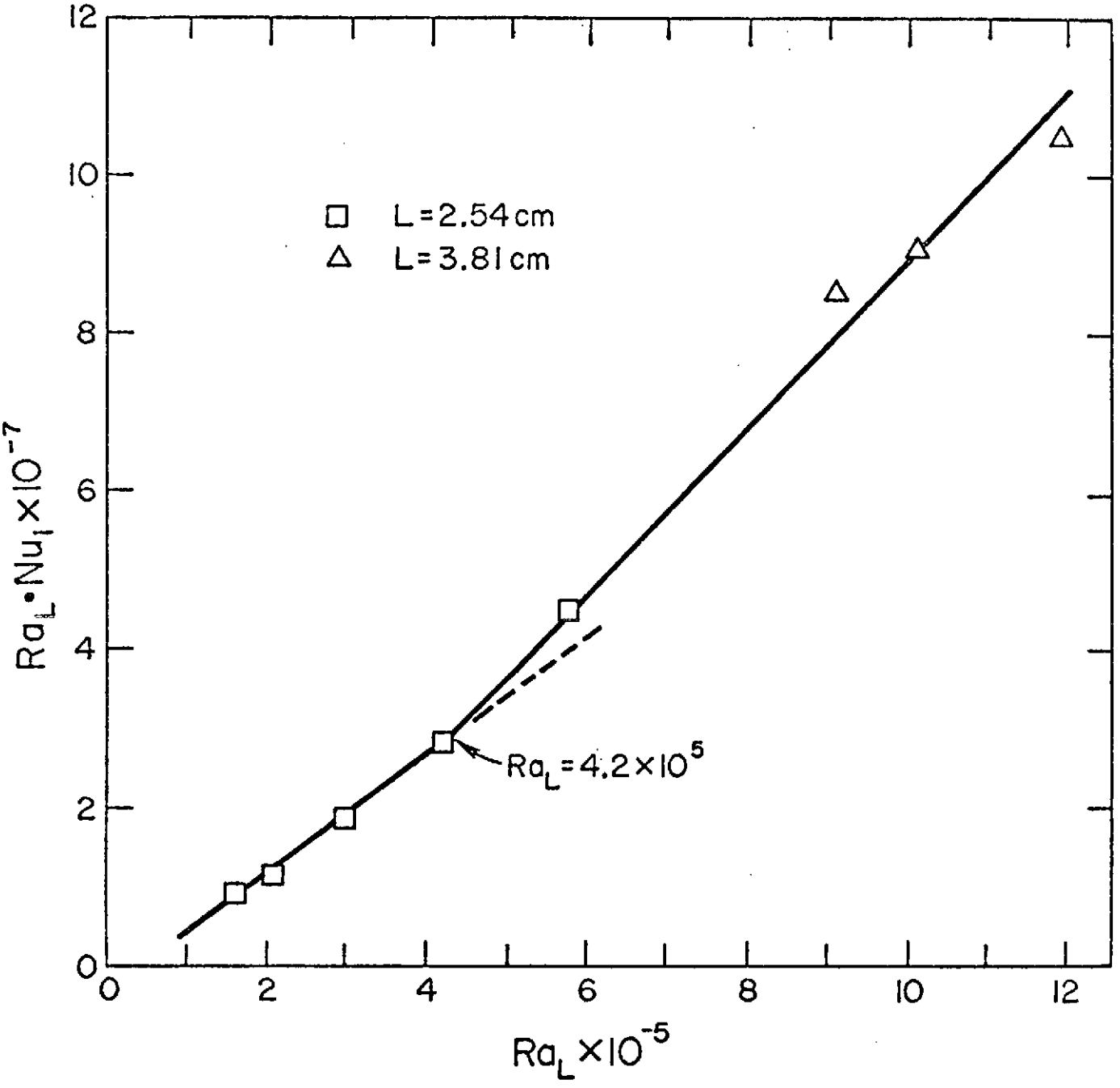

Figure 9. Transition Rayleigh number at $Ra_L = 4.2 \times 10^5$

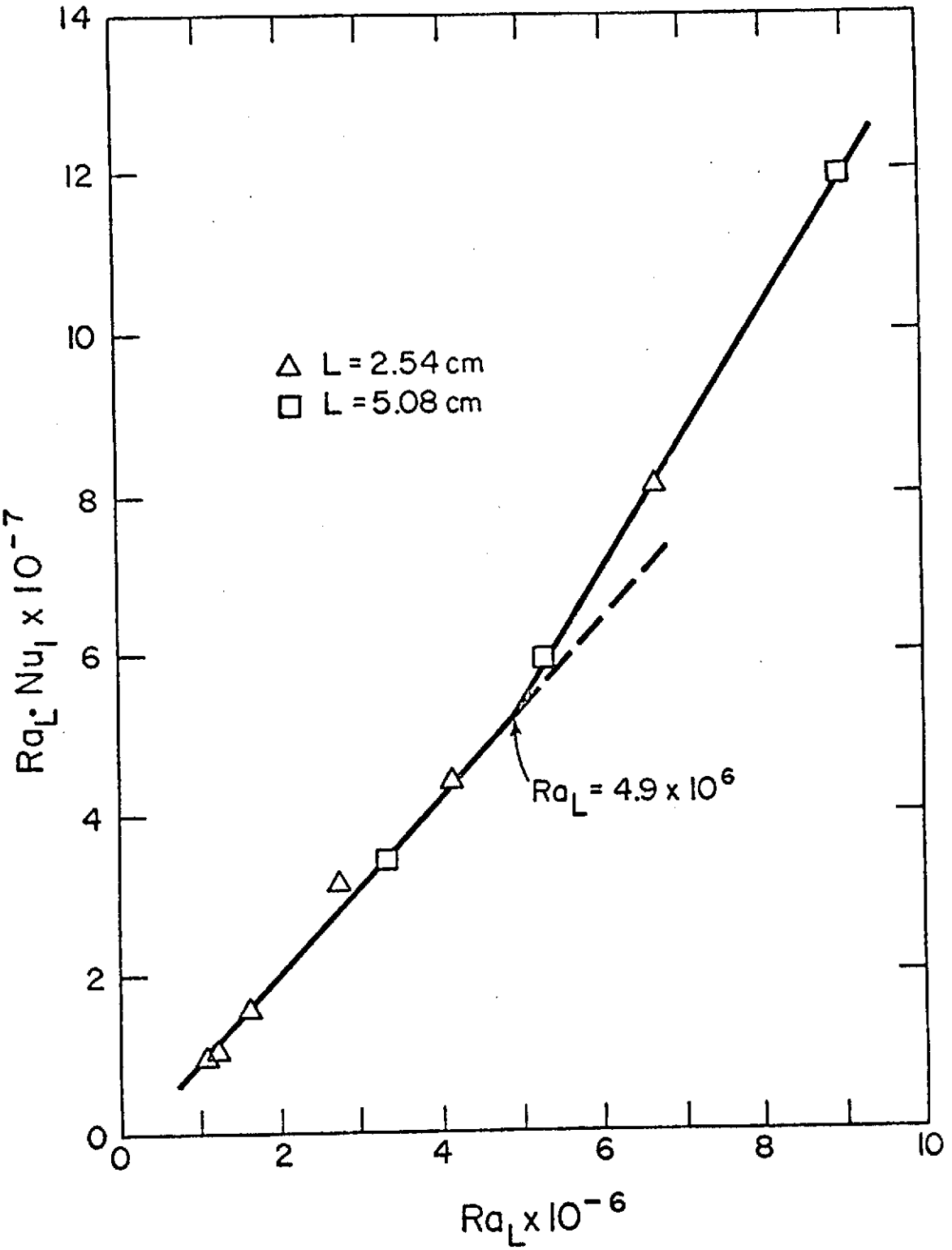

Figure 10. Transition Rayleigh number at $Ra_L = 4.9 \times 10^6$

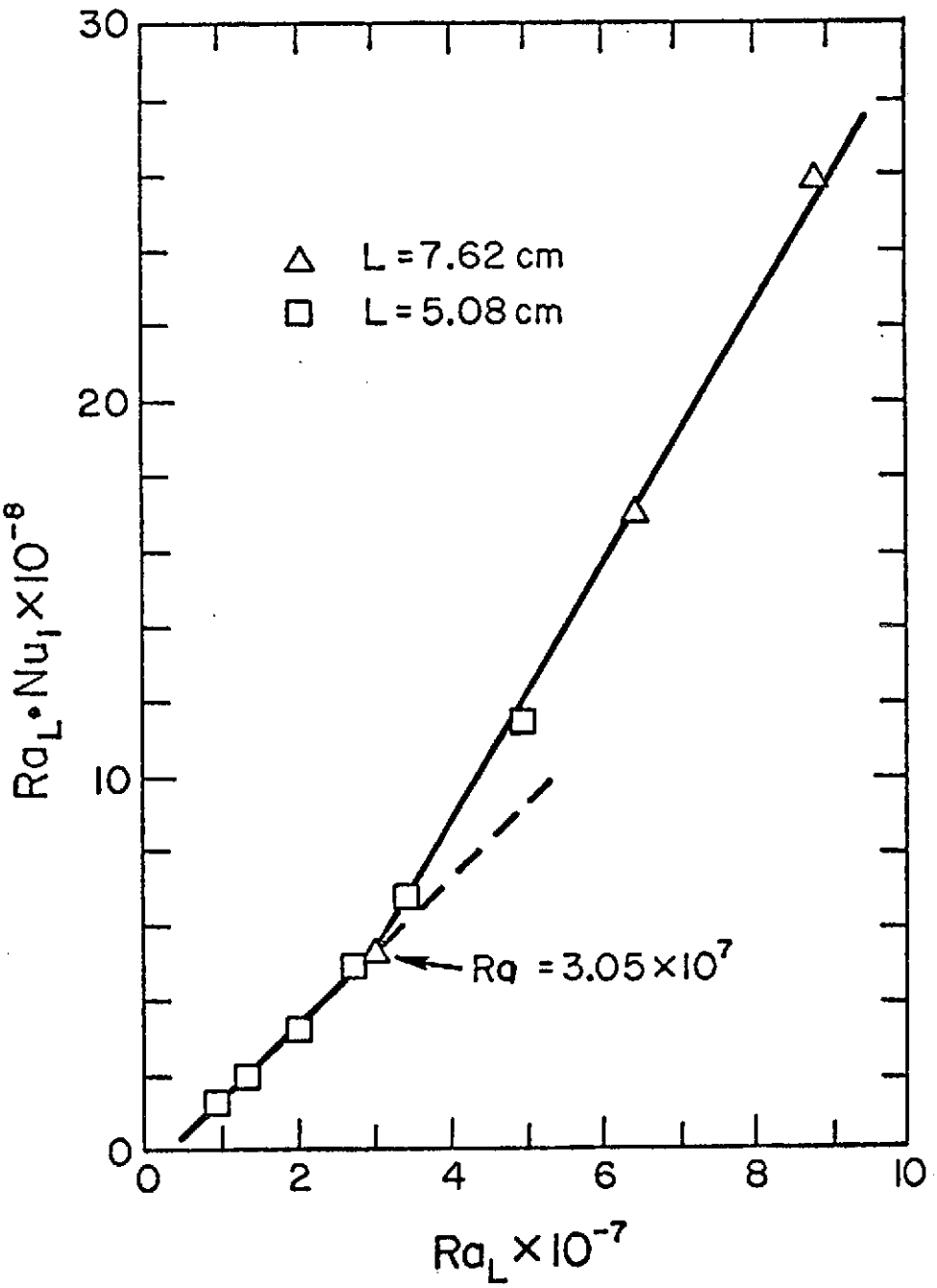

Figure 11. Transition Rayleigh number at $Ra_L = 3.05 \times 10^7$

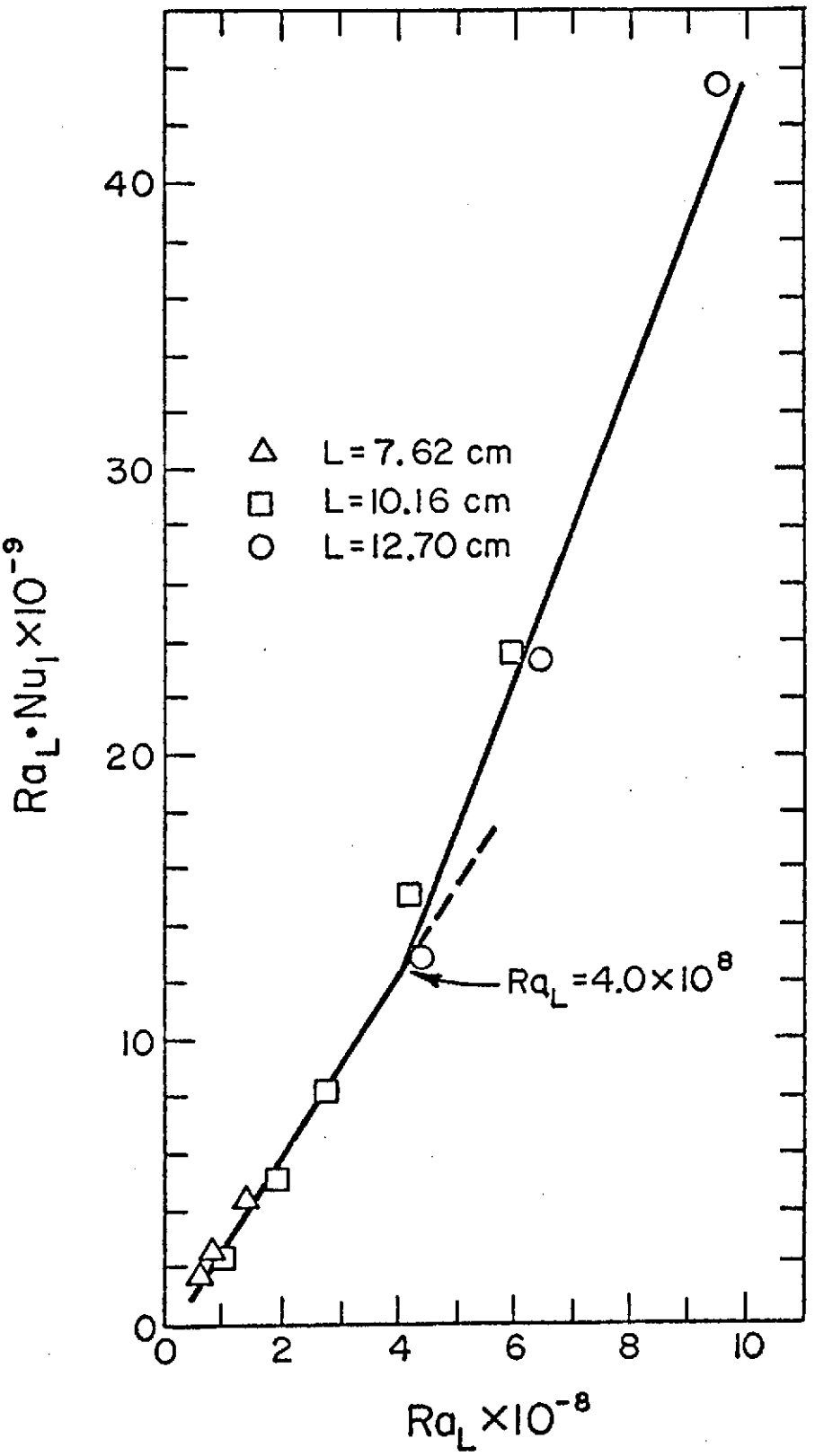

Figure 12. Transition Rayleigh number at $Ra_L = 4.0 \times 10^8$

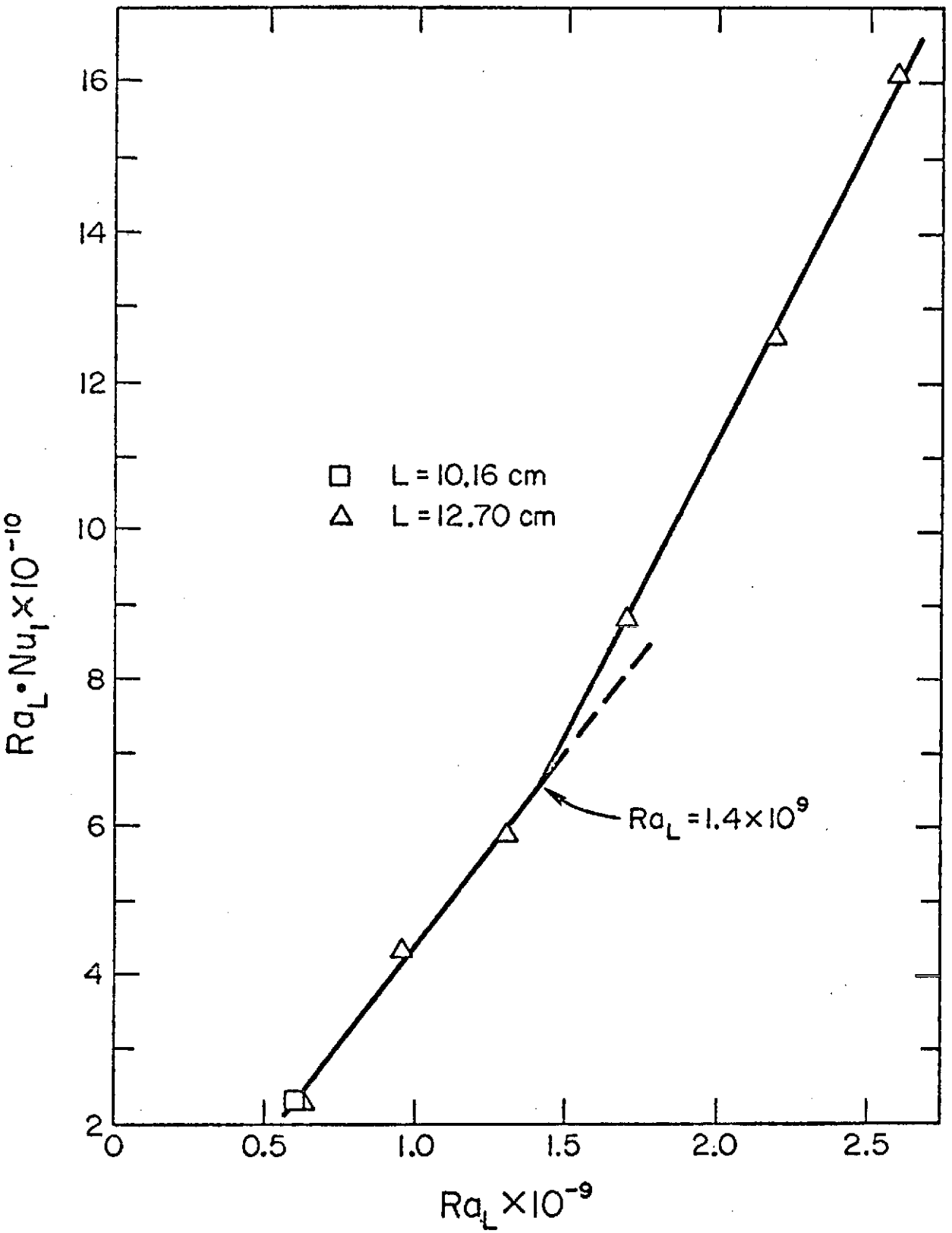

Figure 13. Transition Rayleigh number at $Ra_L = 1.4 \times 10^9$

The transition Rayleigh numbers of this study were obtained using either data for a single plate spacing or data overlapping on both of the transitions from two plate spacings.

4.2 Fluctuating Temperature in Steady Turbulent Convection

After all steady state heat transfer measurements had been completed, a small glass encased thermocouple probe was inserted into the fluid layer through the top boundary plate. The purpose of this probe was to measure the mean and fluctuating component of temperature at various positions in the layer at a given Ra_L. The construction of the probe and the instrumentation used to obtain temperature data are described in Section III.

For steady turbulent convection at a Rayleigh number of 9.3×10^7 ($Ra_L/Ra_{L,c} = 6.7 \times 10^4$ where $Ra_{L,c} = 1386$ [15]), a time trace of fluctuating temperature at various positions in the layer is presented in Figure 14. Rough estimates of the magnitude and duration of temperature fluctuations taken from Figure 14 are given in Table B-V.

If one considers the thermal boundary conditions of the convection chamber, a qualitative picture of the turbulent flow and temperature field can be obtained which is corroborated by the data in Figure 14. The fluid layer in this study is bounded from below by a zero heat flux boundary and from above by a constant temperature plate. Since the fluid is everywhere heated internally, the presence of the cool upper boundary will conduct heat upward through it and in so doing will produce fluid of a generally greater density near it than fluid within the core of the layer. This heavier fluid will become unstable and tend to break away from the upper boundary in the form of eddies or thermals, which will descend into the core of the layer. A similar process of eddy formation and break-away is inhibited, or at least minimized, at the lower boundary due to the absence of a conductively unstable mean temperature profile there. Thus, a turbulent mixing process is established in which cold eddies from the upper boundary plunge into the warm central core and lose their thermal identity largely by diffusion somewhere in the core. Overall mass continuity is maintained in this process by entrainment of warm fluid from the core into the region near the upper boundary, occasional upward migration of warm eddies from the core, and perhaps horizontal flow along the upper surface due to a gross circulation pattern within the layer. In this process, temperature fluctuations should appear greatest and most frequent near the edge of the upper boundary due to the break-away of cold eddies.

From Figure 14, it can be seen that temperature fluctuations are indeed greatest near the upper boundary and gradually diminish with increasing distance from the upper boundary. The frequency of temperature fluctuations also decreased with distance from the upper boundary. By defining the thermal boundary layer thickness at the upper boundary as

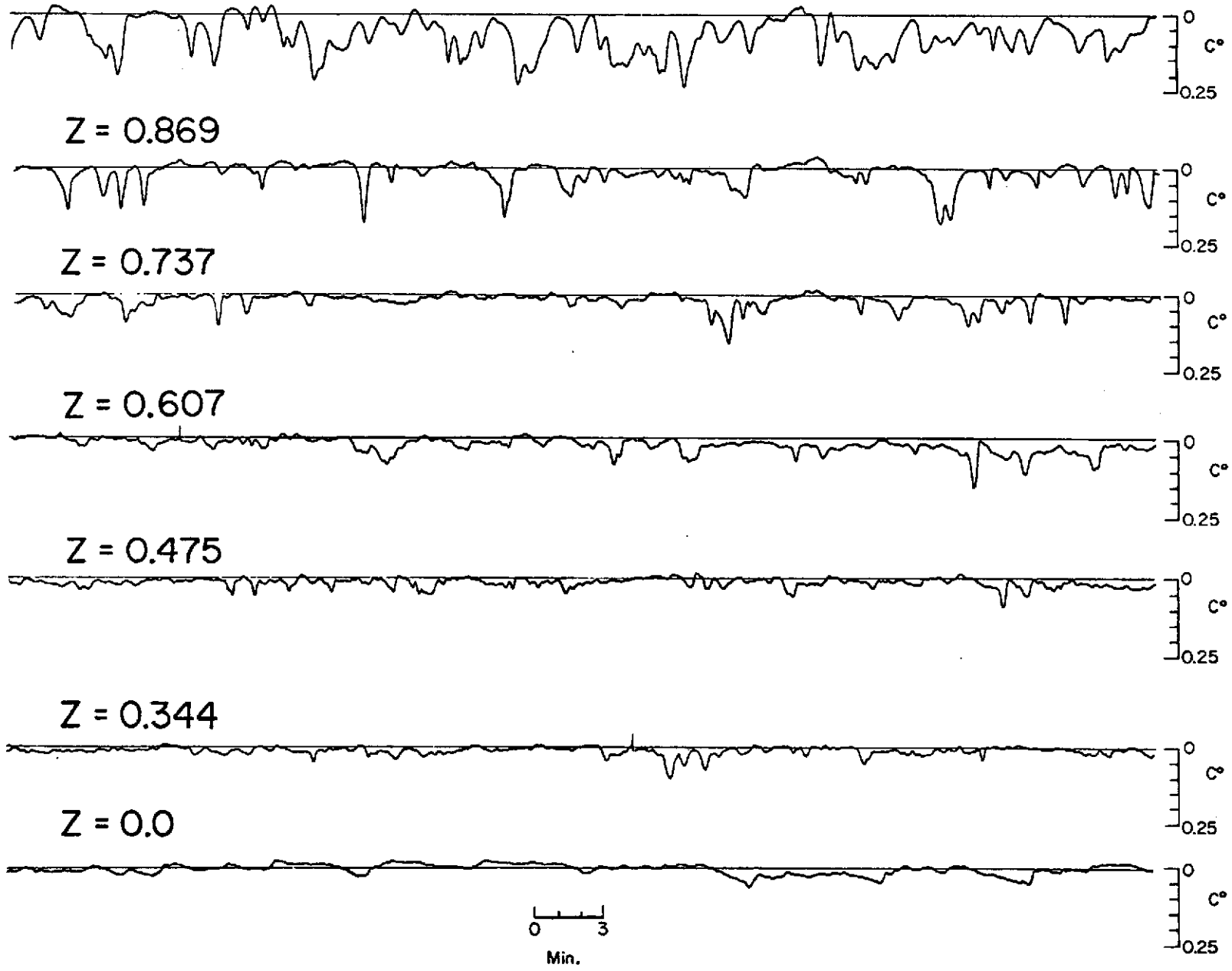

Figure 14. Time trace of fluctuating temperature in steady turbulent convection at $Ra_L = 9.3 \times 10^7$. L = 7.62 cm, $\Delta T = 1.1^{\circ}C$

$$\delta_T = L/Nu_1 ,$$

the correlation for mean heat transfer Eq. (13) gives for $Ra_L = 9.3 \times 10^7$ a nondimensional thermal boundary layer thickness of $\delta_T/L = 0.041$. Thus the edge of the thermal boundary layer on the upper surface is located approximately at $Z = 0.96$. It is just outside this region ($0.87 \lesssim Z \lesssim 0.93$) where temperature fluctuations are the greatest and most frequent for data recorded here. This indicates that the region of most effective eddy mixing occurs at the edge of the thermal boundary layer on the upper surface. The relative absence of large scale temperature fluctuations in the layer core (e.g., $Z < 0.7$) indicates that eddies leaving the upper surface generally lose their thermal identity within a distance of the order of $10 \cdot \delta_T/L$ from the upper boundary.

4.3 Developing Temperature Profiles in Unsteady Convection

A series of runs were conducted to measure the development of temperature in the layer when the Rayleigh number was suddenly changed from a subcritical value to a supercritical value. For a fluid layer with $L = 7.62$ cm, the subcritical Rayleigh number chosen was zero and the supercritical Rayleigh number was 9.3×10^7. The step change in Ra_L was accomplished by switching the power either on or off. Temperature data were gathered by use of the glass encased thermocouple probe in conjunction with a strip chart recorder. Strip chart records of the transient temperature are presented in Appendix C and in reduced form in Figures 15 and 16 and in Tables B-III and B-IV.

In Figure 15, temperature profiles for a step increase in Ra_L ($\Delta Ra_L = 9.3 \times 10^7$) are shown. Here, the mean temperature difference is defined as $T(Z,Fo) - T(Z,0)$, where $T(Z,0)$ is the initial temperature which is the upper boundary temperature, T_1, since the fluid layer was initially isothermal. It was found that for the first few minutes after power had been applied, the temperature profile developed a bulge or over-shoot in the upper 25% of the layer. This behavior is believed to be caused by the thermal inertia of the fluid in the vicinity of the conducting upper boundary. When power is first applied to the layer, it takes some time for the buoyant forces to overcome viscous and inertial forces near the upper boundary. The amount of time required to establish convection near the upper boundary is represented by the time duration of the temperature bulge. In the present study, there was no indication of a temperature bulge for $Fo > 0.0445$. It was found that for all values of Z, steady state had been reached at a $Fo = 0.268$.

After steady state had been reached, the power input to the layer was turned off (i.e., $Ra_L = -9.3 \times 10_2$), and the decay of temperature at the various Z-positions was recorded as a function of time. The reduced results are shown in Figure 16 where Fo indicates the elapsed time from the instant power was turned off. An inspection of the

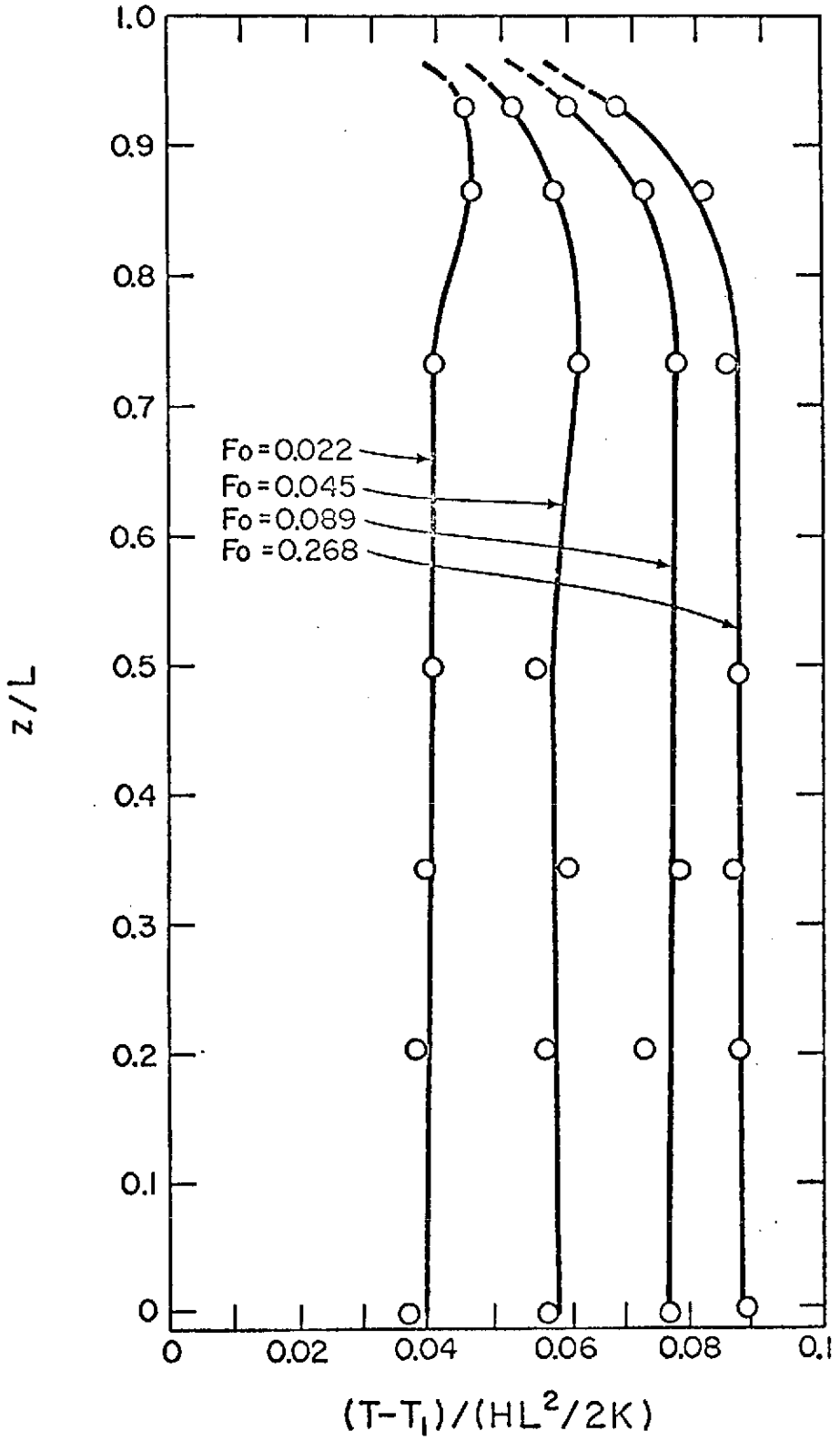

Figure 15. Temperature profiles at various times after the layer is subject to a step increase in power input. Initial Ra_L = 0 and Rayleigh number when power is turned on is 9.3×10^7. L = 7.62 cm.

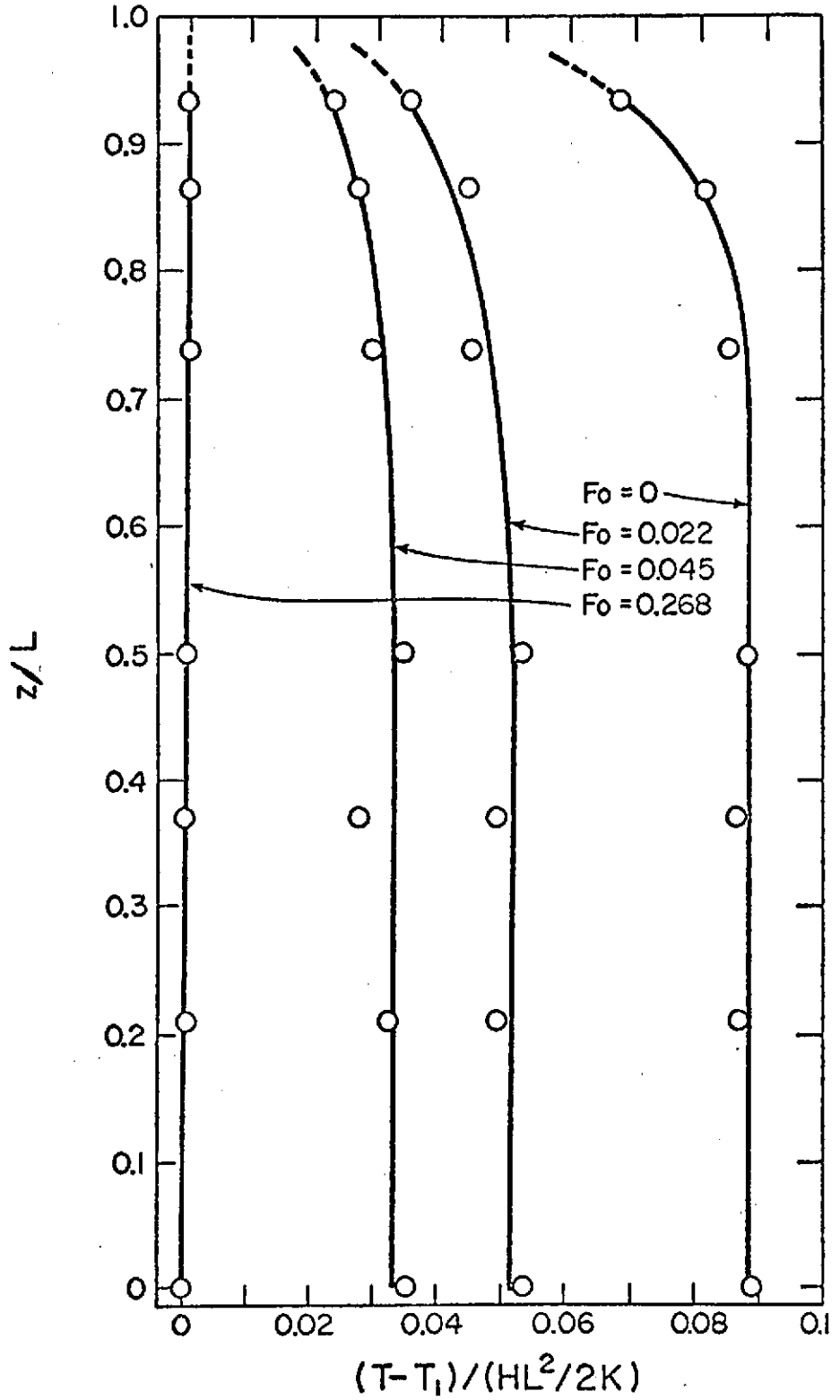

Figure 16. Temperature profiles at various times after the power is suddenly turned off. Steady state Rayleigh number at FO = 0 is 9.3×10^7. L = 7.62 cm

temperature decay data indicated that there was no local temperature bulge (or deficit) as exhibited in the profiles for a step increase in Ra_L.

If the Fourier number of Figure 16 is redefined as 0.268 - Fo, and the reduced temperature profiles for heat-up and cool-down are compared, it can be seen that the two sets of data coincide for the lower 75% of the layer. This may indicate a dynamical similarity between turbulent natural convection with and without heat sources in regions sufficiently far removed from the influence of conductive boundaries.

SECTION V - CONCLUSIONS AND RECOMMENDATIONS FOR FURTHER STUDIES

5.1 Conclusions

In this study, natural convection in a horizontal fluid layer with a uniform volumetric heat source bounded above by an isothermal plate and below by a zero heat flux plate was investigated. Steady state energy transport and, to a limited extent, developing convection were investigated experimentally.

Measurements of the heat transport for Rayleigh numbers up to 1.8×10^6 times the linear stability theory critical value has enabled a correlation for overall heat transfer to be obtained. The Nusselt number at the upper surface was correlated with the Rayleigh number by

$$Nu_1 = 0.305\ Ra_L^{0.239}$$

over the range $1.5 \times 10^5 \leq Ra_L \leq 2.5 \times 10^9$.

By extrapolation of the above correlation to the conduction value of the Nusselt number ($Nu_1=2$), a critical Rayleigh number of 2614 is obtained. This value is within +88.5% of the prediction of linear stability theory [15].

By plotting the energy transport data in the form $Ra_L \cdot Nu_1$ versus Ra_L on linear coordinates, five discrete transitions in heat flux were observed. These transitions were found to occur at Rayleigh numbers of 4.2×10^5, 4.9×10^6, 3.05×10^7, 4.0×10^8, and 1.42×10^9.

The development of mean temperature profiles was investigated for both a step increase and a step decrease in Ra_L. A hysteresis in mean temperature profiles was found between the heat-up and cool-down data; the hysteresis was confined to the upper 25% of the layer.

The magnitude and life span of fluctuating temperature in steady turbulent convection were qualitatively investigated. It was found that at a Rayleigh number of 9.3×10^7, the frequency and magnitude of fluctuations depended on the vertical position in the layer. The largest temperature fluctuations were observed to occur near the outer edge of the thermal boundary layer on the upper surface.

The results of this experimental study have implications for the theory of the thermal state and evolution of planetary bodies. Natural convection driven by radiogenic heat sources is believed to provide the driving force for continental drift. If it is assumed that the convecting region of the mantle is 1,000 km thick and contains all of the Earth's heat sources which have a combined value of $H = 5.8 \times 10^{-7}$ erg/cm^3,

then, with $k = 4 \times 10^5$ erg/cm-s-K, $\alpha = 10^{-2}$ cm^2/s, $\beta = 3 \times 10^{-5}$ K^{-1}, and $\nu = 10^{21}$ cm^2/s, the Rayleigh number appropriate to the upper mantle is approximately 2.2×10^7. If the steady state heat transfer is insensitive to the Prandtl number, the data given in Figure 8 can be used to estimate the temperature differential across this layer; it is found to be about 730°C in this example. This, of course, is significantly less than that determined by models which do not include convective heat transfer.

If, on the other hand, the region is essentially depleted in radioactives due to differentiation during a previous melting-solidification sequence, data of the type presented in Figure 16 could be used to estimate the time for cooling down by solid convection. For the example considered above, the data suggest that the temperature could drop to half the melting temperature in a time $t = (.002)L^2/\alpha = 2.2 \times 10^{18}$ s = 7×10^8 yr.

Further experiments at low Rayleigh numbers and higher Prandtl numbers should provide useful data for modeling the effects of solid convection on planetary thermal histories.

5.2 Recommendations for Further Study

Extensions of the present study are possible using the present apparatus. In the present study the developing and decaying convection was investigated for only one size of step change in Rayleigh number. Developing and decaying convection should be investigated for various step changes in Rayleigh number. In addition, both steady and unsteady convection should be investigated for fluid with large Prandtl number in order to provide data more applicable to problems of geophysical interest.

Other studies which can be conducted with the present apparatus include measurement of steady heat transfer in the laminar (low Rayleigh number) regime and for Rayleigh numbers above 10^{10}. Both Rayleigh regimes are important in both geophysics and engineering. Measurements of overall heat transfer in a layer with a free upper surface would also be desirable since heat generating fluid layers can occur in certain situations in the nuclear technology field.

With minor modifications to the apparatus, other areas of research can be investigated. By operating the electrodes from a programmable power source, a time dependent heat source can be achieved. A more sophisticated analysis of the fluctuating component of turbulent temperature can be accomplished by storing the output of the thermocouple probe on magnetic tape and programming the data for statistical analysis by computer. Such a study would yield the gross spectral features of steady turbulent convection with internal heat sources even with the limited response of the probe.

APPENDIX A

THERMOPHYSICAL PROPERTY VALUES

All of the thermophysical properties of the materials used in the design of the convection cell were taken either from suppliers' literature or from standard tabulated values [20,21,15].

The common thermophysical properties of the silver nitrate solution which served as the heat transfer medium in the convection cell were necessary for calculation of both the Rayleigh and Nusselt numbers. As no attempts were made to precisely control the concentration of silver nitrate from run to run, it was necessary to evaluate these properties for concentration as well as temperature dependence. Computer subroutines used to calculate property values of the aqueous silver nitrate solution were adapted for use in this study from Kulacki [15]. These subroutines used least squares polynomial curve fit when sufficient single parameter data was available; otherwise, linear interpolation was used.

Least squares polynomial fits were developed for both concentration and temperature dependence for density and dynamic viscosity. Values of specific heat and thermal conductivity for pure water were used as functions of temperature alone since sufficient data for concentration dependence does not exist. Use of pure water values for specific heat and thermal conductivity results in errors of the order of $\frac{1}{2}\%$ in these values.

The value of thermal expansion was estimated from information available on the temperature and concentration dependence of solution density. Since the solution density is a smooth function of temperature and concentration, values of $-\frac{1}{\rho}\left[\frac{\partial \rho}{\partial T}\right]$ were estimated by linear interpolation between the value for pure water and the value at 1% dissolved silver nitrate. The value of the derivative $\left[\frac{\partial \rho}{\partial T}\right]$ was evaluated over a temperature interval of 0.10°C at the temperature of the aluminum top plate. Using the value of the coefficient of thermal expansion of pure water would have resulted in at least a 1% error. The accuracy of the value used in this study was estimated to be of the order of $\frac{1}{2}\%$.

Table A-I gives a summary of temperature and concentration dependence of the thermophysical properties of aqueous silver nitrate solution as calculated by the subroutines.

Table A-I - Thermophysical Properties of Aqueous Silver-Nitrate Solution

Property	W	Temperature, °C					
		20	21	22	23	24	25
ρ	0.000	0.998527	0.998235	0.997943	0.997651	0.997359	0.997067
	0.005	0.998569	0.998277	0.997985	0.997693	0.997401	0.997109
	0.010	0.998611	0.998319	0.998027	0.997735	0.997443	0.997151
$\mu \times 10^2$	0.000	1.008658	0.984578	0.961286	0.938764	0.916991	0.895948
	0.005	1.010556	0.986451	0.963135	0.940589	0.918794	0.900331
	0.010	1.012330	0.988208	0.964875	0.942312	0.920499	0.899418
$\beta \times 10^3$	0.000	0.206672	0.217220	0.227564	0.237704	0.247641	0.257375
	0.005	0.206846	0.217375	0.227701	0.237824	0.247745	0.257464
	0.010	0.207020	0.217530	0.227838	0.237944	0.247850	0.257554
C_p	0.000	4.179161	4.178592	4.178076	4.177612	4.177197	4.176831
$k \times 10^2$	0.000	0.597191	0.598869	0.600531	0.602178	0.603805	0.605423

Note that units are: ρ - Density, g/cm^3
μ - Viscosity, g/cm
β - Beta, 1/°C
C_p - Specific heat, W-s/g-°C
k - Conductivity, W/cm-°C

APPENDIX B

EXPERIMENTAL DATA

Table B-I - Steady State Heat Transfer Data

Run No.	L (cm)	P (W)	W (g $AgNO_3$/g H_2O)	ΔT (°C)	$\frac{\Delta T}{HL^2/2k}$	Ra_L	Nu_1	$Ra_L \cdot Nu_1$
24	12.70	175.29	0.0034	2.298	0.032	2.595×10^9	62.16	1.613×10^{11}
25	12.70	148.36	0.0034	2.092	0.034	2.187	57.72	1.263
26	12.70	118.73	0.0034	1.897	0.039	1.719	51.25	8.811×10^{10}
27	12.70	90.18	0.0034	1.638	0.044	1.306	45.25	5.910
9	12.70	66.82	0.0042	1.195	0.043	9.532×10^8	45.61	4.348
10	12.70	45.20	0.0042	1.015	0.055	6.448	36.18	2.333
19	10.16	103.40	0.0034	1.697	0.050	5.940	39.75	2.361
11	12.70	30.38	0.0042	0.833	0.067	4.301	29.85	1.284
20	10.16	73.54	0.0034	1.347	0.056	4.195	35.83	1.503
21	10.16	48.73	0.0034	1.081	0.068	2.767	29.67	8.212×10^9
22	10.16	34.44	0.0034	0.88	0.078	1.944	26.04	5.064
15	7.62	69.51	0.0030	1.099	0.065	1.432	30.51	4.367
23	10.16	17.94	0.0034	0.521	0.089	1.048	22.95	2.405×10^9
16	7.62	49.27	0.0030	0.857	0.071	8.846×10^7	28.14	2.490
17	7.62	35.78	0.0030	0.666	0.075	6.461	26.28	1.698
28	5.08	131.63	0.0037	1.954	0.090	4.881	21.93	1.070
29	5.08	92.80	0.0037	1.542	0.102	3.406	19.59	6.674×10^8
18	7.62	17.27	0.0030	0.500	0.118	3.074	17.04	5.238
30	5.08	76.00	0.0037	1.355	0.109	2.773	18.22	5.052
31	5.08	56.36	0.0037	1.129	0.122	2.037	16.12	3.284
32	5.08	38.02	0.0037	0.843	0.135	1.382	14.76	2.034
33	5.08	24.76	0.0037	0.610	0.150	8.971×10^6	13.39	1.201

Table B-I - Continued

Run No.	L (cm)	P (W)	W (g $AgNO_3$/g H_2O)	ΔT (°C)	$\frac{\Delta T}{HL^2/2k}$	Ra_L	Nu_1	$Ra_L \cdot Nu_1$
36	3.81	57.24	0.0034	1.155	0.164	6.670×10^6	12.18	8.125×10^7
34	5.08	14.56	0.0037	0.430	0.180	5.272	11.23	5.923
37	3.81	35.25	0.0034	0.794	0.184	4.089	10.98	4.490×10^7
35	5.08	9.11	0.0037	0.291	0.195	3.332	10.29	3.430
38	3.81	23.51	0.0034	0.494	0.171	2.696	11.63	3.137
39	3.81	13.60	0.0034	0.329	0.197	1.561	9.87	1.541
40	3.81	10.36	0.0034	0.279	0.219	1.190	8.82	1.049
41	3.81	9.09	0.0034	0.253	0.277	1.054	8.63	9.097×10^6
42	2.54	39.76	0.0034	0.686	0.211	9.078×10^5	9.37	8.505
43	2.54	25.32	0.0034	0.519	0.250	5.752	7.87	4.525
44	2.54	18.67	0.0034	0.448	0.293	4.237	6.75	2.860
12	2.54	13.14	0.0045	0.342	0.318	2.977	6.21	1.848
13	2.54	9.18	0.0045	0.276	0.368	2.079	5.34	1.112
14	2.54	7.20	0.0045	0.206	0.350	1.582	5.71	9.031×10^5

Table B-II - Steady State Heat Transfer Data

Run No.	T_w (°C)	ΔT (°C)	T_∞ (°C)	Power Lost (W)
24	23.558	2.298	24.00	0.189
25	23.482	2.029	23.00	0.408
26	23.175	1.897	25.40	-0.341
27	23.175	1.638	26.10	-0.563
9	22.926	1.195	23.00	0.140
10	22.926	1.015	22.40	0.276
19	22.641	1.697	22.40	0.291
11	22.800	0.833	23.40	-0.049
20	22.532	1.347	24.00	-0.215
21	22.452	1.081	24.00	-0.269
22	22.360	0.881	25.00	-0.588
15	24.805	1.099	22.40	0.790
23	22.914	0.521	24.40	-0.327
16	22.437	0.857	22.20	0.178
17	22.532	0.666	22.40	0.124
28	23.180	1.954	22.40	0.470
29	23.008	1.542	22.40	0.368
18	22.292	0.500	22.80	-0.068
30	22.909	1.355	21.70	0.504
31	22.755	1.129	20.60	0.727
32	22.843	0.843	23.40	-0.036
33	22.790	0.610	23.80	-0.188
36	23.066	1.155	24.30	-0.175
34	22.777	0.430	23.80	-0.216
37	22.987	0.794	24.50	-0.298
35	22.952	0.291	23.30	0.054
38	22.800	0.494	22.70	0.092
39	22.815	0.329	21.70	0.342
40	22.815	0.279	21.70	0.335
41	22.990	0.253	22.40	0.191
42	22.927	0.686	21.70	0.420
43	22.841	0.519	21.70	0.374
44	22.825	0.448	22.40	0.174
12	22.800	0.342	22.40	0.152
13	22.800	0.276	22.40	0.144
14	22.303	0.206	22.40	0.015

Table B-III - Data for Development of Temperature for a Step Increase in Rayleigh Number. Initial $Ra_L = 0$, $\Delta Ra_L = 9.3 \times 10^7$; $L = 7.62$ cm; $T_1 = 22.7°C$

$Z = \frac{z}{L}$	Time (hr)	Fo	$T - T_1$ (°C)	$\frac{T - T_1}{HL^2/2k}$
0.934	0.25	0.022	0.560	0.045
	0.50	0.045	0.655	0.052
	1.00	0.089	0.749	0.060
	3.00	0.268	0.857	0.068
0.868	0.25	0.022	0.574	0.046
	0.50	0.045	0.724	0.058
	1.00	0.089	0.904	0.072
	3.00	0.268	1.012	0.081
0.737	0.25	0.022	0.498	0.040
	0.50	0.045	0.769	0.062
	1.00	0.089	0.959	0.077
	3.00	0.268	1.066	0.085
0.500	0.25	0.022	0.498	0.040
	0.50	0.045	0.701	0.056
	1.00	0.089	0.897	0.071
	3.00	0.268	1.099	0.088
0.344	0.25	0.022	0.496	0.039
	0.50	0.045	0.765	0.061
	1.00	0.089	0.975	0.078
	3.00	0.268	1.080	0.086
0.212	0.25	0.022	0.482	0.038
	0.50	0.045	0.733	0.058
	1.00	0.089	0.911	0.073
	3.00	0.268	1.093	0.087
0.000	0.25	0.022	0.458	0.038
	0.50	0.045	0.722	0.058
	1.00	0.089	0.959	0.077
	3.00	0.268	1.112	0.089

Table B-IV - Data for Development of Temperature for a Step Decrease in Rayleigh Number. Initial $Ra_L = 9.3 \times 10^7$, $\Delta Ra_L = -9.3 \times 10^7$; L = 7.62 cm; $T_1 = 22.7°C$

$Z = \frac{z}{L}$	Time (hr)	Fo	$T - T_{ss}$ (°C)	$\frac{T - T_{ss}}{HL^2/2k}$
0.934	0.25	0.022	0.420	0.033
	0.50	0.045	0.566	0.045
	1.00	0.089	0.709	0.057
	3.00	0.268	0.817	0.065
0.868	0.25	0.022	0.453	0.036
	0.50	0.045	0.668	0.053
	1.00	0.089	0.857	0.069
	3.00	0.268	0.994	0.079
0.737	0.25	0.022	0.489	0.040
	0.50	0.045	0.698	0.056
	1.00	0.089	0.911	0.073
	3.00	0.268	1.053	0.084
0.500	0.25	0.022	0.439	0.035
	0.50	0.045	0.674	0.054
	1.00	0.089	0.897	0.072
	3.00	0.268	1.099	0.088
0.344	0.25	0.022	0.466	0.037
	0.50	0.045	0.733	0.059
	1.00	0.089	0.938	0.075
	3.00	0.268	1.168	0.093
0.212	0.25	0.022	0.474	0.038
	0.50	0.045	0.690	0.055
	1.00	0.089	0.895	0.072
	3.00	0.268	1.093	0.087
0.000	0.25	0.022	0.442	0.035
	0.50	0.045	0.679	0.054
	1.00	0.089	0.884	0.071
	3.00	0.268	1.107	0.088

Table B-V - Magnitude and Time Span of Turbulent Temperature Fluctuations in Steady Convection at $Ra_L = 9.3 \times 10^7$

Z	T'_{avg} (°C)	T'_{max} (°C)	Time Duration (min)
0.934	0.16	0.23	2.0 to 3.0
0.869	0.09	0.18	1.0 to 2.0
0.737	0.06	0.15	0.5 to 1.5
0.607	0.05	0.14	0.5 to 1.5
0.457	0.03	0.10	less than 1
0.344	0.03	0.10	less than 1

Note: T'_{avg} is the arithmetic average taken from a discrete number of observations.

Table B-VI - Time Required for Steady State Conduction Temperature Profile Development in an Initially Quiescent Fluid Layer

Run No.	L (cm)	H (W/cm^3)	Time (hr)
44	2.54	0.00112	1.39
32	5.08	0.00114	7.10
18	7.62	0.00034	14.90
15	7.62	0.00139	18.80
20	10.16	0.00110	35.5
27	12.70	0.00108	58.9

APPENDIX C

STRIP CHART RECORDS OF TEMPERATURE DEVELOPMENT IN UNSTEADY CONVECTION

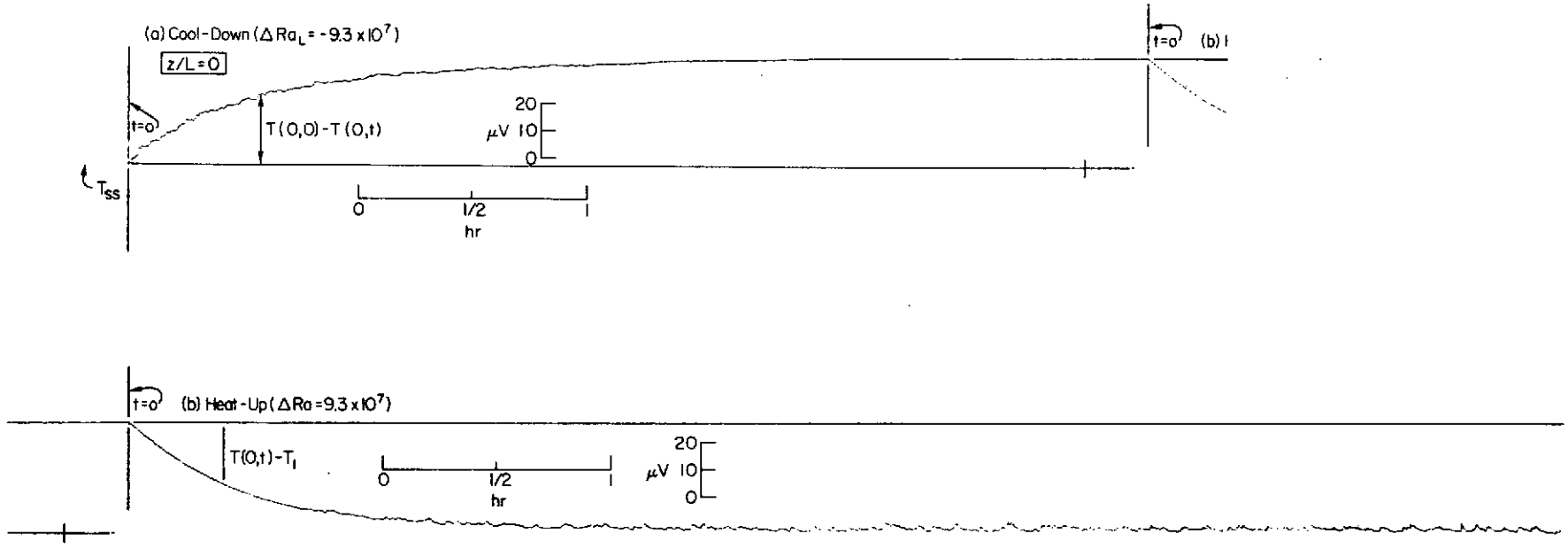

Figure C-1. Strip chart record of transient temperature at z/L = 0
(a) Cool-down, initial $Ra_L = 9.3 \times 10^7$, $\Delta Ra_L = -9.3 \times 10^7$
(b) Heat-up, initial $Ra_L = 0.3 \times 10^7$, $\Delta Ra_L = -9.3 \times 10^7$
(L = 7.62 cm, 41 μV/°C, chart speed = 12.7 cm/hr,
T_i = 22.7°C, power input at $Ra_L = 9.3 \times 10^7$ is 50.9 W)

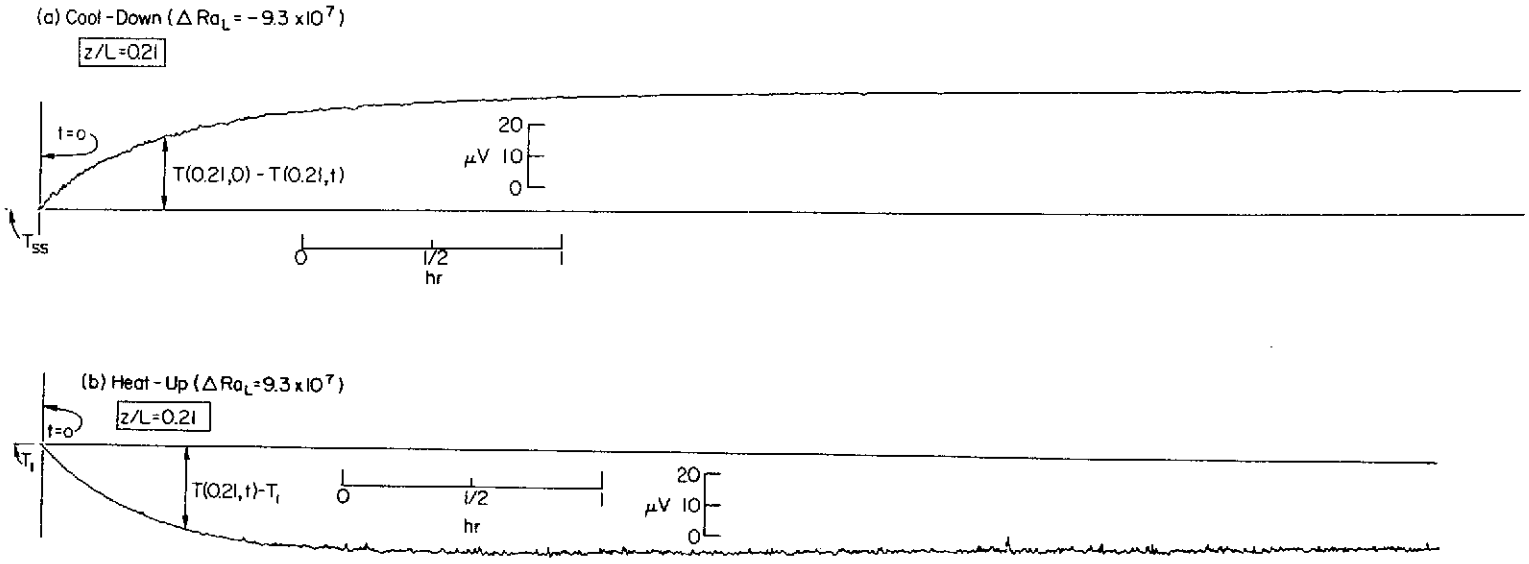

Figure C-2. Strip chart record of transient temperature at z/L = 0.21
(a) Cool-down, initial $Ra_L = 0.3 \times 10^7$ for steady convection, $\Delta Ra_L = -9.3 \times 10^7$
(b) Heat-up, initial $Ra_L = 0$, $\Delta Ra_L = 0.3 \times 10^7$
(L = 7.62 cm, 41 μV/°C, chart speed = 12.7 cm/hr, T_i = 22.7°C, power input at $Ra_L = 9.3 \times 10^7$ is 50.9 W)

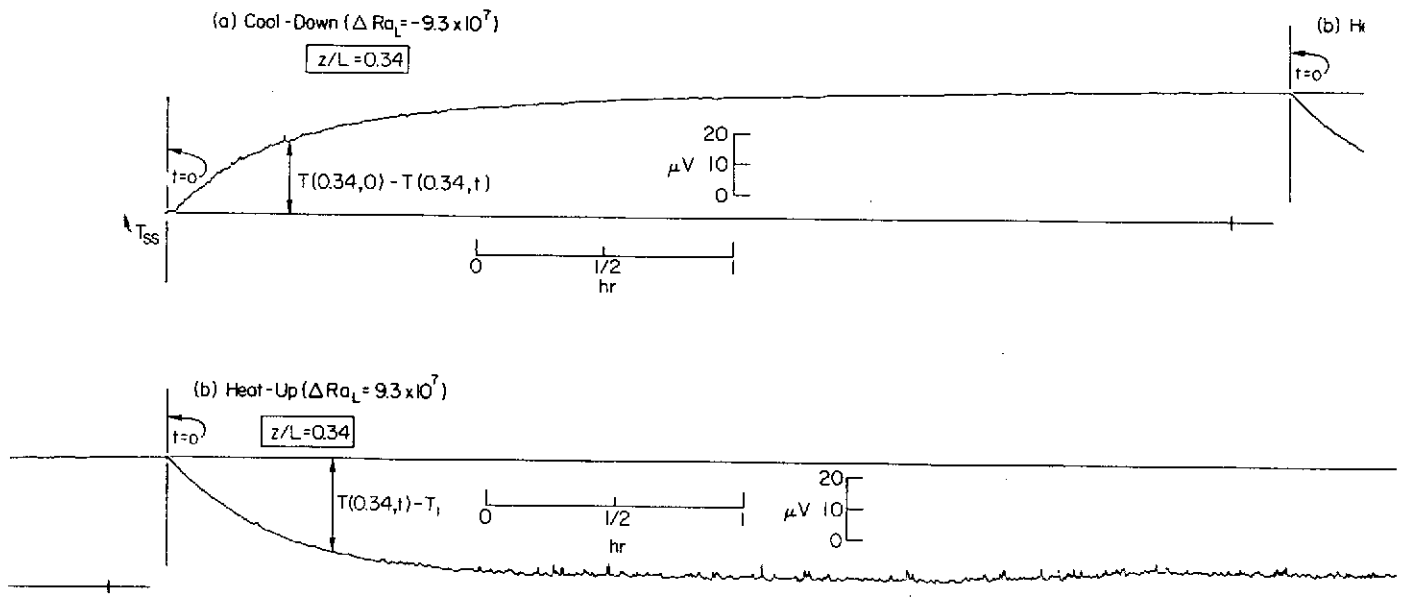

Figure C-3. Strip chart record of transient temperature at z/L = 0.34
(a) Cool-down, initial $Ra_L = 0.3 \times 10^7$ for steady convection, $\Delta Ra_L = -9.3 \times 10^7$
(b) Heat-up, initial $Ra_L = 0$, $\Delta Ra_L = 9.3 \times 10^7$
(L = 7.62 cm, 41 μV/°C, chart speed = 12.7 cm/hr, T_i = 22.7°C, power input at $Ra_L = 9.3 \times 10^7$ is 50.9 W)

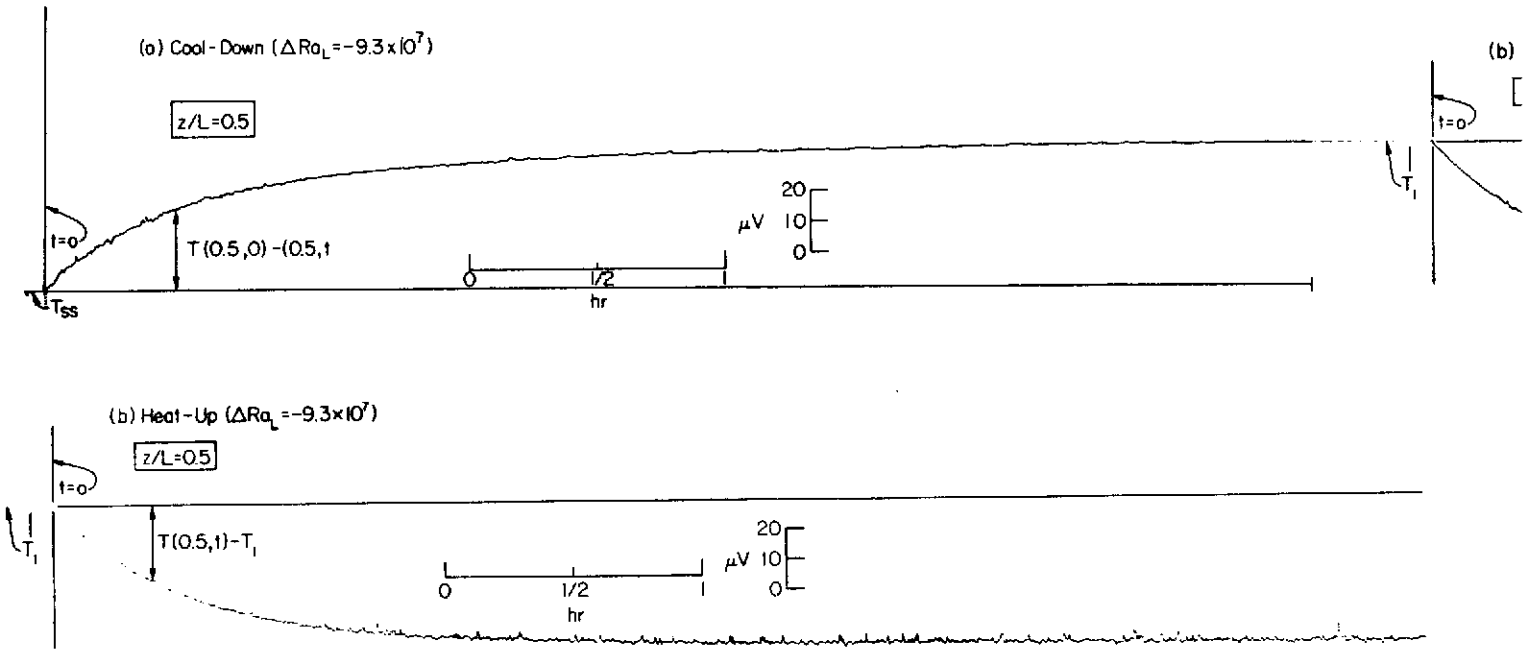

Figure C-4. Strip chart record of transient temperature at z/L = 0.5
(a) Cool-down, initial $Ra_L = 9.3 \times 10^7$ for steady convection, $\Delta Ra_L = 9.3 \times 10^7 = -9.3 \times 10^7$
(b) Heat-up, initial $Ra_L = 0$, $\Delta Ra_L = 9.3 \times 10^7$
(L = 7.62 cm, 41 μV/°C, chart speed = 12.7 cm/hr,
T_i = 22.7°C, power input at $Ra_L = 9.3 \times 10^7$ is 50.9 W)

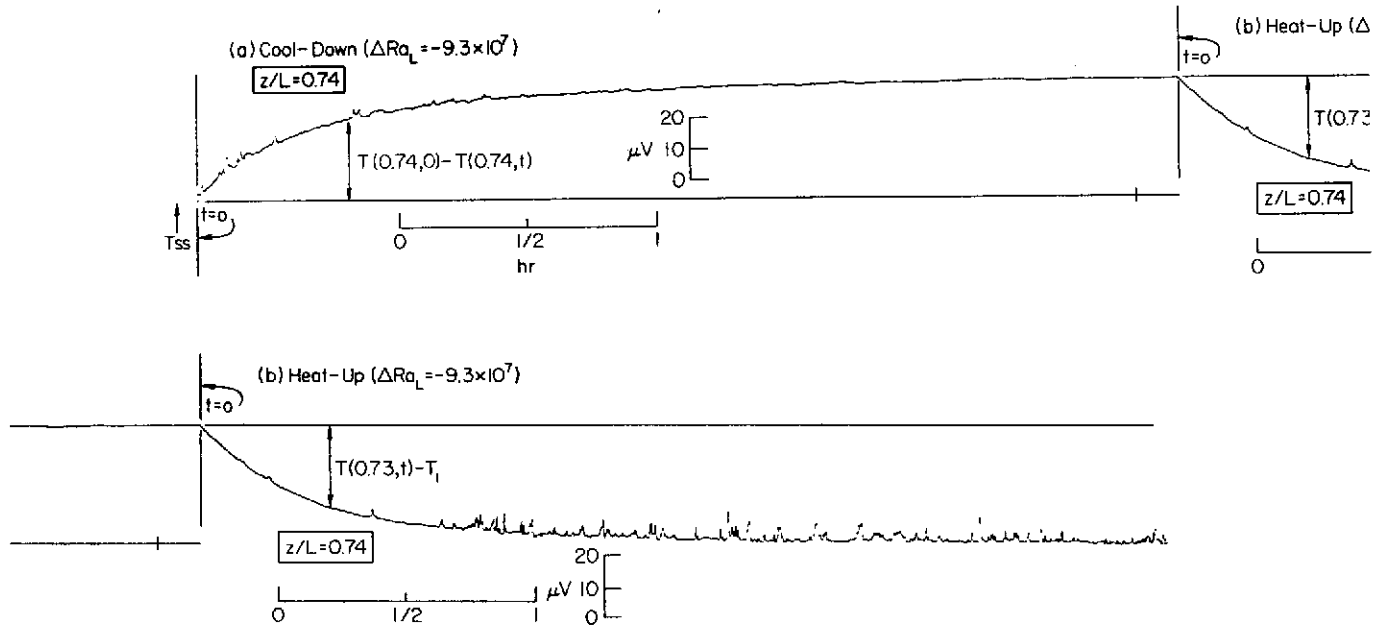

Figure C-5. Strip chart record of transient temperature at z/L = 0.74
(a) Cool-down, initial $Ra_L = 9.3 \times 10^7$ for steady convection, $\Delta Ra_L = -9.3 \times 10^7$
(b) Heat-up, initial $Ra_L = 0$, $\Delta Ra_L = 9.3 \times 10^7$
(L = 7.62 cm, 41 μV/°C, chart speed = 12.7 cm/hr, $T_1 = 22.7°C$, power input at $Ra_L = 9.3 \times 10^7$ is 50.9 W)

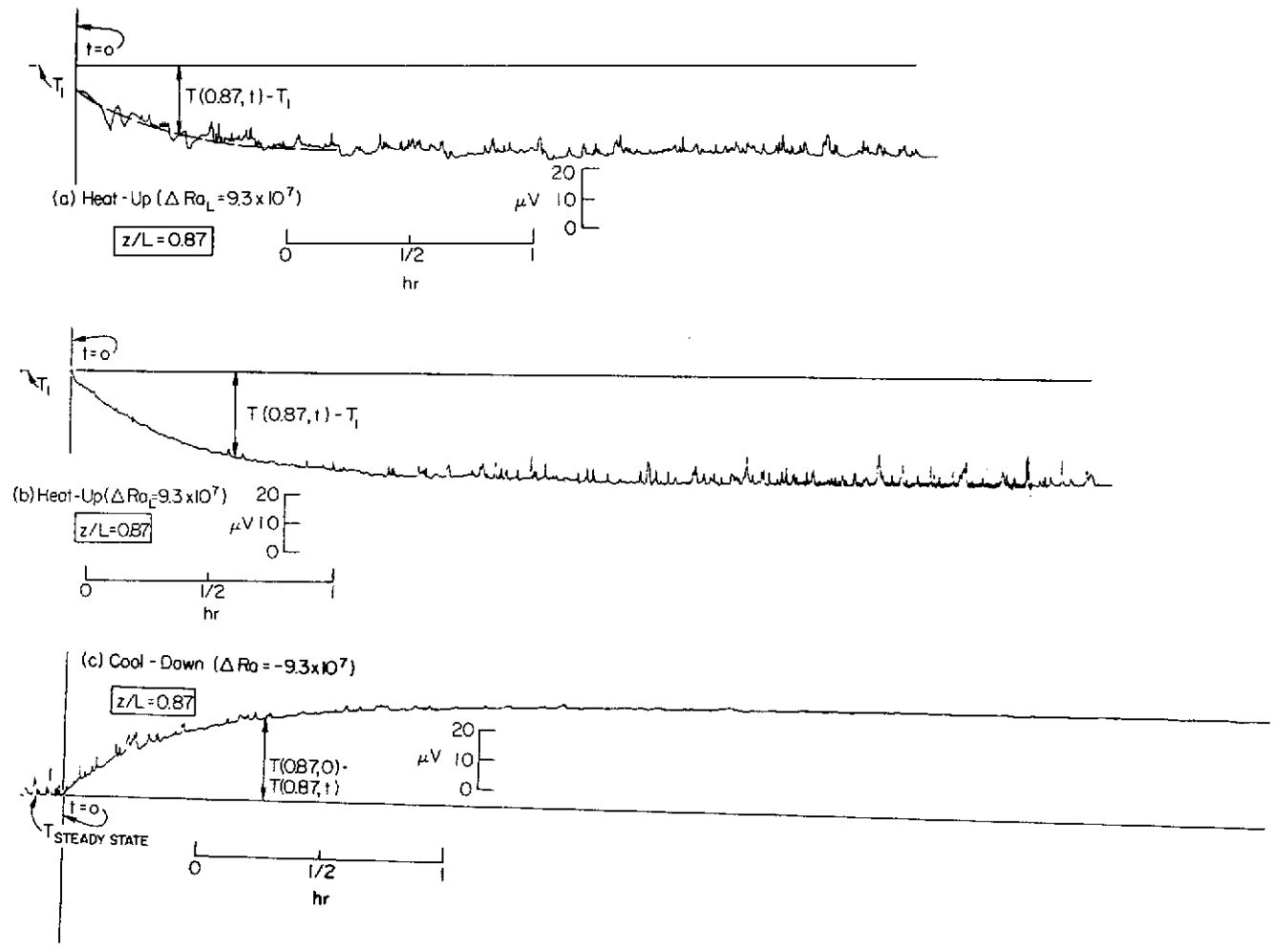

Figure C-6. Strip chart record of transient temperature at z/L = 0.87.
(a) Heat-up, initial Ra_L = 0, $\Delta Ra_L = 9.3 \times 10^7$
(b) Heat-up, initial Ra_L = 0, $\Delta Ra_L = 9.3 \times 10^7$
(c) Cool-down, initial $Ra_L = 9.3 \times 10^7$ for steady convection, $\Delta Ra_L = -9.3 \times 10^7$
(L = 7.62 cm, 41 μV/°C, chart speed = 12.7 cm/hr, T_i = 22.7°C, power input at $Ra_L = 9.3 \times 10^7$ is 50.9 W)

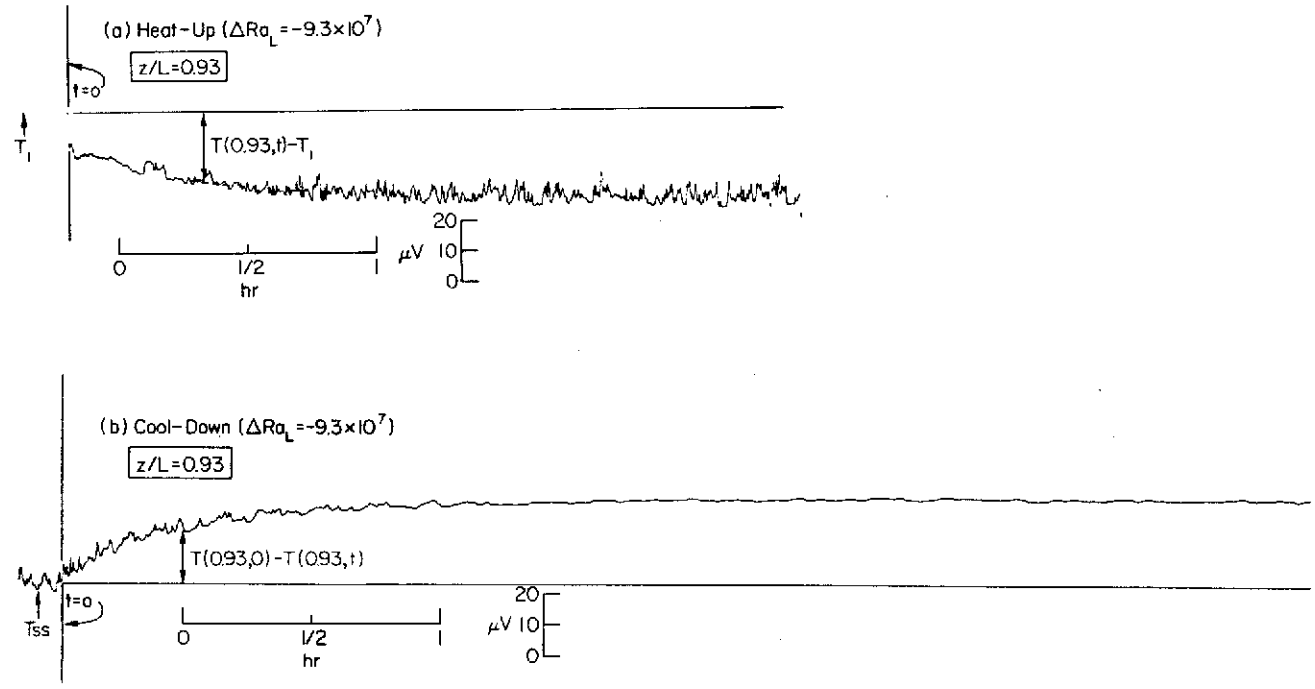

Figure C-7. Strip chart record for transient temperature at z/L = 0.93
(a) Heat-up, initial $Ra_L = 0$, $\Delta Ra_L = 9.3 \times 10^7$
(b) Cool-down, initial $Ra_L = 9.3 \times 10^7$ for steady convection, $\Delta Ra_L = -9.3 \times 10^7$
(L = 7.62 cm, 41 μV/°C, chart speed = 12.7 cm/hr, T_1 = 22.7°C, power input at $Ra_L = 9.3 \times 10^7$ is 50.9 W)

APPENDIX D

ANALYSIS OF EXPERIMENTAL ERRORS

Because of uncertainties in the parameters used to calculate the Rayleigh number and Nusselt number these dimensionless quantities are subject to a certain amount of error. Both accidental and systematic forms of errors are present.

The accidental error in the project was eliminated in the experiments by taking those measurements which were repeatable several times and taking arithmetic mean values for those readings. Assuming that this method is sufficient to eliminate the accidental error it was assumed that all error resulted from systematic error.

The systematic errors include uncertainties in the thermophysical properties of the electrolyte solution, readings of the wattmeter transducer, convection cell geometrical dimensions, temperature measurements and the power lost through the bottom plate and sidewalls. Each form of error will be considered in turn. It will be assumed that no error results from concentration gradients of the salt, since the flow is highly turbulent, nor from any temperature dependence which might exist in the three-dimensional heat source. It is also assumed that the convection cell is perfectly aligned with the horizontal axis of the earth.

Applying the law of summation of fractional errors [22], the fractional error in the Rayleigh number is

$$f_{Ra} = f_{properties} + f_{geometric} + f_{power}$$

and the fractional error in the Nusselt number is

$$f_{Nu} = f_{properties} + f_{geometric} + f_{power} + f_{temperature}$$

The estimated uncertainty in the thermophysical property values are given in Appendix A.

The Mylar covering of the aluminum top plate had an uncertainty of 0.00127 cm which when added to the uncertainty of the Plexiglas plate spacers, 0.00127 cm resulted in an uncertainty of 0.00254 cm in the fluid layer depth, L. The horizontal dimension of the convection cell is known to within 0.0127 cm. An error of 0.5% was used for all geometrical measurements.

The combined uncertainties in the thermophysical properties and geometrical factors produced an uncertainty of 4 to 5% in the experimental Rayleigh number and 1 to 2% in the experimental Nusselt number.

The error of the wattmeter transducer was rated at 0.25% of reading. Allowing for error of reading the millivolt output of the transducer with the multimeter, the estimated uncertainty in power consumption was 0.5%.

The calculated value of the energy transported through the bottom plate and sidewalls was less than 1% of the measured power input for each run. It is not possible to systematically determine the amount of error in this calculated energy loss because nominal property values supplied by the manufacturer were used in the calculation. Thus, the actual value of energy transported through the top plate was taken to be within 1% of the calculated value.

The uncertainties in the thermocouple output, potentiometer reading and conversion from emf to degrees Centigrade resulted in the error of the measured temperature to be 1%. This gives the most probable error in the temperature difference of 1.5%.

Summing all fractional errors, the error in the Rayleigh number is 5 to 6% and the error in the Nusselt number is 3.5 to 4.5%.

REFERENCES

1. The Earth's Mantle, (ed.) T. F. Gaskell, Academic Press, New York, 1961.

2. Runcorn, S. K., "Convection Currents in the Earth's Mantle," Nature, 195, 1248 (1962).

3. Tozer, D. C., "Heat transfer in convection currents," Proc. Roy. Soc. (London), A258, 252 (1966).

4. Orowan, E., "The Origin of the Oceanic Ridges," Sci. Amer., (November 1969).

5. Schubert, G., Turcotte, D. L., and Oxburgh, E. R., "Stability of Planetary Interiors," Geophys. J., 18, 441 (1969).

6. Bethe, H. A., "Energy Production in Stars," Science, 161, 541 (1968).

7. Mihaljan, J., "A Rigorous Exposition of the Boussinesq Approximation Applicable to a Thin Layer of Fluid," Astrophys. J., 136, 1126 (1967).

8. Rayleigh, Lord, "On Convection Currents in a Horizontal Layer of Liquid When the Higher Temperature Is on the Underside," Phil. Mag., 32, 529 (1916).

9. Tritton, D. J. and Zarraga, M. N., "Convection in Horizontal Layers With Heat Generation. Experiments," J. Fluid Mech., 34 (1), 21, (1967).

10. Benard, H., "Les Tourbillons Celluaires Dans Une Nappe Liquide, Methods Optiques D'Observation ed D'Enregistrement," J. de Physique, 10, 254 (1901).

11. Krishnamurty, R., "Finite Amplitude Convection With Changing Mean Temperature. Part 2, An Experimental Test of the Theory," J. Fluid Mech. 33 (3), 457 (1968).

12. Whitehead, J. A. and Chen, M. M., "Thermal Instability and Convection of a Thin Fluid Layer Bounded by a Stable Stratified Region," J. Fluid Mech., 40 (3), 549 (1970).

13. Schwab, J. A. and Schwiderski, E. W., "Convection Experiments with Electrolytically Heated Fluid Layers," J. Fluid Mech., 48, 703 (1971).

14. Kulacki, F. A. and Goldstein, R. J., "Natural Convection in a Horizontal Fluid Layer With Uniform Volumetric Energy Sources," J. Fluid Mech., 55 (2), 271 (1972).

15. Kulacki, F. A., Thermal Convection in a Horizontal Fluid Layer With Uniform Volumetric Energy Sources, Ph.D. Dissertation, University of Minnesota, 1971.

16. Fiedler, H. E. and Wille, R., "Turbulente, Freie Konvektion in Einer Horizontalen Flussigkeitsschicht mit Volumen-Warmequelle," Paper NC 4.5, Proc. Fourth Int. Heat Trans. Conf., Paris-Versailles, 1970.

17. Nagle, M. E., "Natural Convection Energy Transport in a Horizontal Fluid Layer With Volumetric Heat Sources," M. Sc. Thesis, Department of Mechanical Engineering, The Ohio State University, March, 1974.

18. Malkus, V. W. R., "Discrete Transitions in Turbulent Convection," Proc. Roy. Soc. (London), A225, 185 (1954).

19. Willis, G. E. and Deardorff, J. W., "Confirmation and Renumbering of the Discrete Heat Flux Transitions of Malkus," Phys. Fluids, 10, 1861 (1967).

20. American Cyanamid Company, Plastics Catalog, Product Bulletin No. 454, Wallingford, Conn.

21. Chemical Rubber Company, Handbook of Chemistry and Physics, 51st Edition, 1970.

22. Topping, J., Errors of Observation and Their Treatment, Chapman and Hall, London, 1955.